

## Chapter 2

# Acoustic Solitons

The need to consider nonlinear terms in the different equations of solid state physics has long been realised. Ignoring lattice anharmonicity, it is impossible to explain the thermal expansion and heat conductivity of a solid body. Previously, in the framework of perturbation theory, only a small nonlinearity was taken into account, one that occasionally caused a loss of key features, determined by the nonlinearity of the problem. Anharmonicity of molecular lattice vibration reveals itself especially strongly in so-called quasi-one-dimensional crystals – systems composed of parallel chains the size of the molecular diameter (the nearest-neighbor distance inside one chain is substantially smaller than the distance between the atoms in different chains).

### 2.1 Fermi–Pasta–Ulam Problem (FPU)

A rigorous consideration of the nonlinear vibration of molecular chains began with the work of Fermi, Pasta, and Ulam (FPU) [1]. For the first time, a computational study of nonlinear dynamics was carried out. In a chain with harmonic interaction potential, the normal modes of vibration are mutually independent variables. The modes do not interact with each other (thermalisation of one mode does not lead to thermalisation of other modes). FPU considered that, if a nonlinearity were introduced into the interaction, an energy flux would occur, leading eventually to equipartition of energy, in accord with the principles of statistical mechanics. They thus set out to confirm this in a computational experiment, but it turned out that only a small part of the energy was redistributed. Such systems have been shown to return recurrently to their initial states.

Let us consider a one-dimensional chain of molecules, arranged along the  $x$  axis at interval  $a$ . All molecules in the chain are supposed to be of unitary mass  $M$ , and the interaction of molecules is described by a unified potential  $V(r)$ , where  $r$

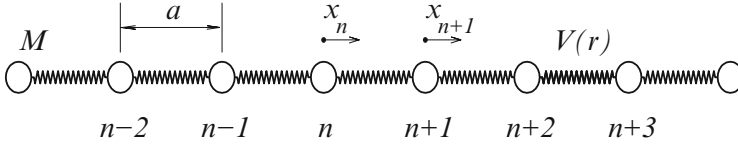


**Fig. 2.1** Model of a one-dimensional molecular chain

is the displacement of a molecule with respect to its equilibrium position ( $r = 0$  in equilibrium position). We also assume that only nearest-neighboring molecules interact with each other. A schematic view of this system is shown in Fig. 2.1. In the ground state, the  $n$ th molecule in the chain has coordinate  $x = na$ . Let  $x_n(t)$  be the displacement of the  $n$ th molecule with respect to its equilibrium position at time  $t$ . Then the Hamiltonian of the system takes the form

$$\mathcal{H} = \sum_{n=-\infty}^{+\infty} \left[ \frac{1}{2} M \dot{x}_n^2 + V(r_n) \right], \quad (2.1)$$

where a dot over  $x_n$  denotes differentiation with respect to time  $t$ , and  $r_n = x_{n+1} - x_n$  is the elongation of the  $n$ th bond of the chain. The following equations of motion correspond to the Hamiltonian of the system (2.1):

$$M \ddot{x}_n = F(x_{n+1} - x_n) - F(x_n - x_{n-1}), \quad n = 0, \pm 1, \pm 2, \pm 3, \dots, \quad (2.2)$$

where the function  $F(r) = dV/dr$ .

If the force resulting from the bond deformation is proportional to the bond strain as in Hooke's law, i.e.,  $F(r) = Kr$ , the string is said to be linear and the molecular interaction is described by the harmonic potential

$$V(r) = \frac{1}{2} Kr^2, \quad (2.3)$$

where  $K$  is the rigidity of the intermolecular interaction. For an anharmonic potential, the rigidity is  $K = V''(0)$ . In the case of a harmonic interaction potential, the equations of motion (2.2) are linearised:

$$M \ddot{x}_n = K(x_{n+1} - 2x_n + x_{n-1}), \quad n = 0, \pm 1, \pm 2, \pm 3, \dots \quad (2.4)$$

Any linear combination of solutions of equations (2.4) is also a solution of this system.

Consider a finite chain composed of  $N + 2$  links ( $n = 0, 1, 2, \dots, N, N + 1$ ) with fixed end particles ( $x_0 \equiv 0, x_{N+1} \equiv 0$ ). Then Eqs. (2.4) have  $N$  linearly independent solutions (linear modes):

$$\begin{aligned} x_n^{(l)}(t) &= A_l \sin \frac{\pi l n}{N+1} \cos(\omega_l t + \delta_l) , \\ \omega_l &= 2\sqrt{K/M} \sin \frac{\pi l}{2(N+1)} , \quad l = 1, 2, \dots, N . \end{aligned} \quad (2.5)$$

The amplitudes  $A_l$  and phases  $\delta_l$  of the modes do not depend on time and are defined by initial conditions. The modes do not interact with each other, so the linear chain is not ergodic.

In his early academic career, Fermi was engaged in a study of the ergodic problem, and when computers came on the scene, he returned to this theme because it was thought that one particular problem might be solved with the aid of a computer. He thought that, if a nonlinear term were to be introduced into the force acting between particles in a chain, the modes would exchange energy, causing the system to reach a statistical equilibrium state in which energy is uniformly distributed over the linear modes. It was this expectation that FPU believed would be confirmed by a computational simulation.

They modeled the chain dynamics using three potentials. The first potential involved a cubic anharmonic term (the FPU  $\alpha$ -potential):

$$V(r) = K \left( \frac{1}{2} r^2 - \frac{1}{3} \alpha r^3 \right) , \quad (2.6)$$

the second, quartic anharmonic term (the FPU  $\beta$ -potential):

$$V(r) = K \left( \frac{1}{2} r^2 + \frac{1}{4} \beta r^4 \right) , \quad (2.7)$$

and the third, a piecewise continuous quadratic function:

$$V(r) = \begin{cases} \frac{1}{2} K r^2 , & \text{if } |r| < r_0 , \\ \frac{1}{2} K' r^2 + \frac{1}{2} (K - K') r_0^2 , & \text{if } |r| \geq r_0 . \end{cases} \quad (2.8)$$

The results turned out to be qualitatively similar for all the potentials.

FPU considered a chain with fixed end points and a number of links  $N$  equal to 32 or 62. To model this system, one must put  $n = 0, 1, \dots, N+1$ ,  $x_0 \equiv 0$ , and  $x_{N+1} \equiv 0$  in the equations of motion (2.2). At the initial time, the lowest mode was excited, so the initial condition was

$$x_n(0) = A \sin \frac{\pi n}{N+1} , \quad x_n'(0) = 0 , \quad n = 0, 1, \dots, N+1. \quad (2.9)$$

The numerical integration of the equations of motion (2.2) with initial condition (2.9) showed that, after some time, almost all the energy was back in the initial mode. This is the so-called FPU recurrence phenomenon.

Computational simulation occasionally leads to utterly unexpected results, and the FPU recurrence phenomenon was one of these. Furthermore, this result was repeatedly confirmed. One may assert that, if the energy is low and the initial shape of the wave is sufficiently smooth, the recurrence phenomenon occurs. Norman Zabusky [2, 3] summarised the results in the empirical equation which determines the recurrence time at an initial excitation of the lowest mode:

$$t_r = \frac{0.44N^{3/2}t_1}{\sqrt{|\alpha|A}}, \quad (2.10)$$

where  $t_1 = 2N\sqrt{K/M}$  is the time taken by the wave of long wavelength to travel back and forth along the chain of  $N$  particles with fixed ends (or the period of the wave going round the closed chain of  $2N$  particles). It was shown further that the recurrence phenomenon is related to the presence of localised solitary waves (solitons) in the chain, while (2.10) is associated with the characteristics of the soliton motion [4].

The FPU recurrence phenomenon is also observed in the case of a finite chain with periodic boundary conditions. Let us consider in detail this phenomenon occurring in the closed chain. For convenience of numerical modeling, we introduce the following dimensionless variables: displacement  $u_n = x_n/a$ , time  $\tau = t\sqrt{K/M}$ , and energy  $H = \mathcal{H}/Ka^2$ . Then the cyclic chain of  $N$  particles can be described by the dimensionless Hamiltonian

$$H = \sum_{n=0}^{N-1} \left[ \frac{1}{2} u_n'^2 + U(\rho_n) \right], \quad (2.11)$$

where the prime denotes differentiation with respect to the dimensionless time  $\tau$ , while  $\rho_n = u_{n+1} - u_n$  is the relative displacement, and the dimensionless interaction potential  $U(\rho_n) = V(a\rho_n)/Ka^2$  is normalised according to the conditions

$$U(0) = 0, \quad U_\rho(0) = 0, \quad U_{\rho\rho}(0) = 1. \quad (2.12)$$

The Hamiltonian (2.11) leads to the following finite system of equations of motion:

$$u_n'' = F(u_{n+1} - u_n) - F(u_n - u_{n-1}), \quad n = 0, 1, \dots, N-1, \quad (2.13)$$

where the function  $F(r)$  is defined here as  $F(r) = dU/d\rho$ , while  $n+1 = 0$  if  $n = N-1$  and  $n-1 = N-1$  if  $n = 0$ .

The linear mode of the cyclic chain takes the form

$$u_n(\tau) = A \exp[i(qn - \omega\tau)], \quad (2.14)$$

where  $A$ ,  $q \in [0, 2\pi]$ , and  $\omega = 2 \sin(q/2)$  are the amplitude, wavenumber, and frequency of the mode, respectively. In the case of the cyclic chain of  $N$  molecules,

the wavenumbers can only take  $N$  values, viz.,

$$q_k = 2\pi k/N, \quad k = 0, 1, \dots, N-1.$$

The amplitude of the  $k$ th mode is defined by the equation

$$A_k = \frac{1}{\sqrt{N}} \sum_{n=0}^{N-1} u_n \exp(-iq_k n). \quad (2.15)$$

It follows from this equation that  $A_{N-k} = \bar{A}_k$ . For the chain with harmonic interaction potential, the amplitude of the mode is constant, as opposed to the chain with anharmonic potential, for which the amplitude depends on time according to

$$A_k' = \frac{1}{\sqrt{N}} \sum_{n=0}^{N-1} u_n' \exp(-iq_k n). \quad (2.16)$$

In the case of a harmonic chain, the energy of the  $k$ th mode is described by the equation  $E_k = \omega_k^2 |A_k|^2$ , where the mode frequency is specified by the relation  $\omega_k = 2 \sin(q_k/2)$ . Let us define the energy of the mode for an anharmonic chain as  $E_k = (|A_k'|^2 + \omega_k^2 |A_k|^2)/2$  and integrate the system (2.13) with the initial condition corresponding to the linear mode of wavenumber  $q_1$ :

$$u_n(0) = A \sin \frac{2\pi n}{N}, \quad u_n'(0) = 0. \quad (2.17)$$

Note that, given the initial condition, the problem is equivalent to the dynamics of a chain of  $N/2 - 1$  links with fixed ends, when the first linear mode is excited.

From now on, we write the FPU  $\beta$ -potential of intermolecular interaction in the form

$$U(\rho) = \frac{1}{2}\rho^2 + \frac{1}{4}\beta\rho^4. \quad (2.18)$$

Furthermore, let us fix the amplitude of the mode  $A = 0.1$ , but allow the anharmonicity parameter  $\beta$  to change.

The equations of motion are linear when  $\beta = 0$ , so all the energy of the initial excitation remains in the given mode. The rest of the modes are not excited in this scenario. When  $\beta > 0$ , the modes can exchange energy. The numerical simulation showed that a portion of the energy drifts from the first mode, but periodically recurs to it (Fig. 2.2a left), whence the initial shape of the wave is recovered. This is the FPU recurrence phenomenon. The greater the anharmonicity of the interaction potential, the higher the amplitude of the change in the mode energy. For strong nonlinearity, the periodic energy exchange between the modes becomes unstable and recurrence does not proceed, resulting in the energy spreading

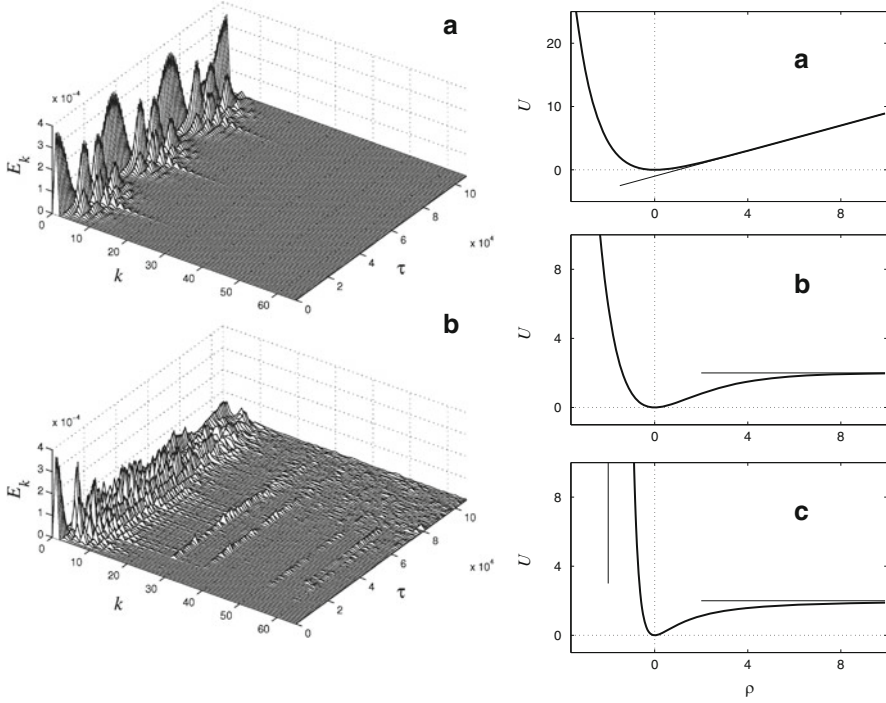


**Fig. 2.2** *Left:* Energy exchange between the linear modes in the anharmonic cyclic chain ( $N = 132$ ) for initial excitation of only the first mode  $k = 1$  ( $q = 2\pi/N$  and the amplitude of the mode is  $A = 0.1$ ). The dependence of the energy distribution  $E_k$  over the linear modes of the chain on the time  $\tau$  is also shown ( $k$  is the mode number). **(a)** Weak nonlinearity  $\beta = 1,000$ . Periodic recurrence of the energy to the initial mode occurs (the FPU recurrence phenomenon). **(b)** Strong nonlinearity  $\beta = 2,000$ . The energy is redistributed over the other modes. *Right:* Interstitial potentials  $U(\rho)$ . **(a)** Toda potential (2.34) with  $b = 1$ . **(b)** Morse potential (2.41) with  $\epsilon = 2, \beta = 0.5$ . **(c)** Lennard-Jones potential (4,2) (2.42) with  $\epsilon = 2, a = 2$ . *Lines* show the asymptotics of the potentials

among the various modes (Fig. 2.2b left). The same effect takes place if one fixes the nonlinearity parameter and changes the mode amplitude. The FPU recurrence phenomenon is observed only when the mode amplitude is less than an arbitrary threshold value.

For the recurrence phenomenon to exist, the initial wave shape must be smooth (the wavelength of the mode  $\lambda = 2\pi/q \gg 1$ ). Excitation of a single short wavelength mode in the anharmonic chain leads to fast thermalisation of the rest of the modes. The recurrence phenomenon is associated with the existence of stable, elastically-interacting solitary waves in the chain, i.e., solitons. At an energy below the threshold value, the initial deformation of the chain transforms into solitons which are periodically assembled together, forming the initial shape of the wave.

## 2.2 Solitary Waves

Consider an anharmonic chain. The dimensionless Hamiltonian of the chain takes the form (2.11), where the sum runs over all integer indices ( $n = 0, \pm 1, \pm 2, \dots$ ). Taking into account the normalization conditions (2.12), the dimensionless interaction potential  $U(\rho) = V(a\rho)/Ka^2$  can be expanded in a series:

$$U(\rho) = \frac{1}{2}\rho^2 - \frac{1}{3}\alpha\rho^3 + \frac{1}{4}\beta\rho^4 + \dots, \quad (2.19)$$

where  $\alpha = -U^{(3)}(0)/2$  and  $\beta = U^{(4)}(0)/6$  are nonlinearity parameters. The equations of motion take the form (2.13) with  $n = 0, \pm 1, \pm 2, \dots$  and

$$F(\rho) = \rho - \alpha\rho^2 + \beta\rho^3 + \dots. \quad (2.20)$$

In the case of small displacements, one can neglect all the anharmonic terms in the series (2.19). As a result, we obtain the harmonic potential  $U(\rho) = \rho^2/2$  and the equations of motion become linear:

$$u_n'' = u_{n+1} - 2u_n + u_{n-1}, \quad n = 0, \pm 1, \pm 2, \dots, \quad (2.21)$$

The solution of (2.21) can be represented as a sum of linear waves

$$u_n(\tau) = A \exp i(qn - \omega\tau), \quad (2.22)$$

where  $A, q \in [-\pi, \pi]$ , and  $\omega = 2 \sin(q/2)$  are the wave amplitude, wavenumber, and wave frequency, respectively. The wavelength  $\lambda = 2\pi/q$  tends to infinity as  $q \rightarrow 0$  and the wave velocity is

$$s(q) = \frac{\omega(q)}{q} = \frac{\sin(q/2)}{q/2}$$

which tends to the dimensionless velocity of the long-wavelength phonon,  $s_0 = 1$ .

In the case of anharmonic potential, the linear wave solution (2.22) is no longer the explicit solution of the infinite-dimensional system of equations of motion (2.13). Let us search for the solution of this system as a solitary wave of constant shape, i.e.,

$$u_n(\tau) = u(n - s\tau),$$

where  $s$  is the dimensionless velocity of the wave, and the wave shape  $u(n)$  depends smoothly on the discrete variable  $n$ . To use the continuum approximation, the following parameter must be small:

$$\mu = \max_n \left| \frac{du(n)}{dn} \right|.$$

This parameter describes the reciprocal width of the solitary wave (soliton). It follows that all the derivatives obey the relationship  $d^m u/dn^m = O(\mu^n)$ . Therefore in the continuum approximation, the following partial differential equation corresponds to the discrete equations of motion (2.13):

$$(1 - s^2)u_{zz} + \frac{1}{12}u_{zzzz} + \frac{1}{360}u_{zzzzzz} - \alpha \left( 2u_z u_{zz} + \frac{1}{3}u_{zz} u_{zzz} + \frac{1}{6}u_z u_{zzzz} \right) 11 \\ + \beta \left( 3u_z^2 u_{zz} + u_z u_{zzz} + \frac{1}{4}u_{zz}^2 + \frac{1}{4}u_z^2 u_{zzzz} \right) + O(\mu^6) = 0 ,$$

where  $z = n - s\tau$  is the continuous wave variable approximating the discrete variable  $n$ . Considering only the terms smaller than  $\mu^5$ , this equation takes the form

$$(1 - s^2)u_{zz} + \frac{1}{12}u_{zzzz} - 2\alpha u_z u_{zz} + 3\beta u_z^2 u_{zz} = 0 . \quad (2.23)$$

Let us change from the absolute displacement  $u(z)$  to a relative displacement  $\rho = u_z$ . Then (2.23) takes the form

$$(1 - s^2)\rho_z + \frac{1}{12}\rho_{zzz} - 2\alpha\rho\rho_z + 3\beta\rho^2\rho_z = 0 . \quad (2.24)$$

For a solitary wave, the state of the chain at infinity must be the ground state, and therefore

$$\rho, \rho_z, \rho_{zz} \longrightarrow 0 \quad \text{as } z \rightarrow \pm\infty . \quad (2.25)$$

Integrating (2.24) once and considering the boundary conditions (2.25) leads to the well-known Boussinesq equation:

$$(1 - s^2)\rho + \frac{1}{12}\rho_{zz} - \alpha\rho^2 + \beta\rho^3 = 0 . \quad (2.26)$$

This has explicit analytical solutions only for the FPU  $\alpha$ -potential (the cubic anharmonic potential,  $\beta = 0$ ):

$$\rho(z) = -A/\cosh^2(\mu z) , \quad A = 3(s^2 - 1)/2\alpha , \quad \mu = \sqrt{3(s^2 - 1)} , \quad (2.27)$$

and the FPU  $\beta$ -potential (the quartic anharmonic potential,  $\alpha = 0$ ):

$$\rho(z) = A/\cosh(\mu z) , \quad A = \pm\sqrt{2(s^2 - 1)/\beta} , \quad \mu = \sqrt{12(s^2 - 1)} . \quad (2.28)$$

The soliton solution of the Boussinesq equation (2.24) has been studied by Toda and Waddati [5]. In the chain with cubic anharmonicity ( $\beta = 0$ ), the soliton solution (2.27) exists for any value of the anharmonicity parameter  $\alpha \neq 0$  and



velocity  $s > 1$ . The bell-shaped function (2.27) describes a region of localized compression (extension) in the chain for the anharmonicity parameter  $\alpha > 0$  ( $\alpha < 0$ ). This region moves along the chain, retaining its shape with velocity  $s > s_0$ , where  $s_0 = 1$  is the dimensionless velocity of sound (the velocity of the long-wavelength phonon) in the chain. Such localized excitation of the chain is called a *supersonic acoustic soliton*.

In terms of the absolute displacement, the acoustic soliton is described by the following solution of the equations of motion for the chain:

$$u_n(\tau) = \frac{A}{\mu} \left\{ 1 - \tanh [\mu(n - s\tau)] \right\}. \quad (2.29)$$

Since the displacement  $u_n \rightarrow -2A/\mu$  as  $n \rightarrow -\infty$  and  $u_n \rightarrow 0$  as  $n \rightarrow +\infty$ , the chain moves as a whole to the right through a distance  $2A/\mu$  (total compression of the chain).

The energy of the acoustic soliton (2.29) in the chain with cubic anharmonicity is given by the relation

$$\begin{aligned} E &= \sum_{n=-\infty}^{+\infty} \left[ \frac{1}{2} u_n'^2 + U(\rho_n) \right] = \int_{-\infty}^{+\infty} \left[ \frac{1}{2} (1 + s^2) \rho^2(z) - \frac{1}{3} \alpha \rho^3(z) \right] dz \\ &= \frac{1}{\mu} \left[ \frac{2}{3} (1 + s^2) A^2 + \frac{16}{45} \alpha A^3 \right], \end{aligned} \quad (2.30)$$

and the root-mean-square width of the soliton is defined by

$$L = 2 \left( \frac{1}{R} \sum_{n=-\infty}^{+\infty} n^2 \rho_n \right)^{1/2} = 2 \left[ \frac{1}{R} \int_{-\infty}^{+\infty} z^2 \rho(z) dz \right]^{1/2} = \frac{\pi}{\sqrt{3}\mu}, \quad (2.31)$$

where the total compression of the chain is

$$R = \sum_{n=-\infty}^{+\infty} \rho_n = \int_{-\infty}^{+\infty} \rho(z) dz = \frac{2A}{\mu}.$$

It follows from (2.27), (2.30), and (2.31) that the energy of the acoustic soliton  $E(s)$  and its amplitude  $A(s)$  steadily increase when its velocity increases, while the soliton width  $L(s)$  steadily decreases: as  $s \rightarrow 1$ ,  $E(s) \searrow 0$ ,  $A(s) \searrow 0$ , and  $L(s) \nearrow \infty$ , and as  $s \rightarrow \infty$ ,  $E(s) \nearrow \infty$ ,  $A(s) \nearrow \infty$ , and  $L(s) \searrow 0$ .

Equations (2.27) and (2.29)–(2.31) have been obtained in the continuum approximation, which can only be used if the soliton width  $L(s) \gg 1$ . The continuum approximation gives acceptable results for  $L(s) = \pi/\mu(s)\sqrt{3} = \pi/3\sqrt{s^2 - 1} > 5$ , that is, for  $s < \sqrt{1 + (\pi/15)^2} = 1.022$ . At high velocities, the continuum approximation cannot be applied, but this does not mean that the discrete equations of motion do not admit soliton solutions for  $s > 1.022$ . Indeed, soliton solutions

exist for all values of the velocity  $s > 1$ . To obtain the explicit shape of the soliton with width comparable to the lattice spacing ( $L \sim 1$ ), the numerical Eilbeck–Flesh pseudospectral method [6, 7] can be used.

In a chain with quartet anharmonicity ( $\alpha = 0$ ), the acoustic soliton exists only for positive anharmonicity  $\beta > 0$ . According to (2.28), the soliton solution exists for each value of the velocity  $s > 1$ . By symmetry of the interaction potential, there are two similar solutions: soliton and antisoliton, with amplitudes  $A > 0$  and  $A < 0$ , respectively. In a localization region of the acoustic soliton (antisoliton), compression (extension) of the chain takes place.

At a fixed velocity  $s > 1$ , the two types of supersonic soliton have the same energy

$$\begin{aligned} E &= \sum_{n=-\infty}^{+\infty} \left[ \frac{1}{2} u_n'^2 + U(\rho_n) \right] = \int_{-\infty}^{+\infty} \left[ \frac{1}{2} (1 + s^2) \rho^2(z) + \frac{1}{4} \beta \rho^4(z) \right] dz \\ &= \frac{1}{\mu} \left[ (1 + s^2) A^2 + \frac{1}{3} \beta A^4 \right], \end{aligned} \quad (2.32)$$

the same absolute value of total chain compression (extension)

$$R = \left| \sum_{n=-\infty}^{+\infty} \rho_n \right| = \left| \int_{-\infty}^{+\infty} \rho(z) dz \right| = \frac{A\pi}{\mu},$$

and the same width

$$L = 2 \left( \frac{1}{R} \sum_{n=-\infty}^{+\infty} n^2 \rho_n \right)^{1/2} = 2 \left[ \frac{1}{R} \int_{-\infty}^{+\infty} z^2 \rho(z) dz \right]^{1/2} = \frac{\pi}{\mu}. \quad (2.33)$$

It follows from (2.28), (2.32), and (2.33) that the energy of the acoustic soliton  $E(s)$  and its amplitude  $A(s)$  steadily increase when its velocity increases, while the soliton width  $L(s)$  steadily decreases: as  $s \rightarrow 1$ ,  $A(s) \searrow 0$ ,  $E(s) \searrow 0$ , and  $L(s) \nearrow \infty$ , and as  $s \rightarrow \infty$ ,  $E(s) \nearrow \infty$ ,  $A(s) \nearrow \infty$ , and  $L(s) \searrow 0$ .

The continuum approximation used here for the chain with quartet anharmonicity is applicable when

$$L(s) = \frac{\pi}{\mu(s)} = \frac{\pi}{\sqrt{12(s^2 - 1)}} > 5,$$

that is, when  $s < \sqrt{1 + \pi^2/300} = 1.016$ . Yet, using the pseudospectral method [6, 7], it can be shown that the discrete equations of motion (2.13) have a soliton solution for all supersonic values of the velocity  $s > 1$ . However, the explicit soliton solution cannot be obtained analytically. It can only be obtained numerically, although with any desired precision, for velocities  $s > 1$ . An explicit analytical equation can only be obtained in the case of the chain with the Toda potential [8].

## 2.3 Solitons in the Toda Chain

A nonlinear chain with exponential interaction has been studied by Toda and Waddati [5] and Toda [9–13]. The results of the study are most comprehensively represented in his book [8]. It has been shown that the equations describing the dynamics of such a lattice admit explicit  $N$ -soliton solutions. These equations also have an infinite set of integrals of motion, and constitute a completely integrable Hamiltonian system which can be solved by the inverse scattering method.

The dimensionless Toda potential, normalized by the conditions (2.12), has the form

$$U(\rho) = \frac{1}{b} \left\{ \rho + \frac{1}{b} [\exp(-b\rho) - 1] \right\}, \quad (2.34)$$

where  $b > 0$  is the anharmonicity parameter. The potential is given in Fig. 2.2a (right). The potential increases exponentially as  $b^{-2} \exp(-b\rho)$  when  $\rho \rightarrow -\infty$  and linearly as  $\rho/b - 1/b^2$  when  $\rho \rightarrow +\infty$ . The chain with the interaction potential (2.34) is called the Toda chain. The parameter  $b$  in the potential describes its anharmonicity. For small displacements,  $b\rho \ll 1$ , the interaction potential takes the form

$$U(\rho) = \frac{1}{2}\rho^2 - \frac{1}{6}b\rho^3 + \dots$$

The dimensionless equations of motion (2.13) are

$$u_n'' = \frac{1}{b} [\exp(-b\rho_{n-1}) - \exp(-b\rho_n)], \quad n = 0, \pm 1, \pm 2, \dots \quad (2.35)$$

Taking into account the relative displacements  $\rho_n = u_{n+1} - u_n$ , the equation of motion (2.35) can be rewritten in terms of the relative displacements:

$$\rho_n'' = -\frac{1}{b} [\exp(-b\rho_{n-1}) - 2\exp(-b\rho_n) + \exp(-b\rho_{n+1})], \quad n = 0, \pm 1, \pm 2, \dots \quad (2.36)$$

It can readily be shown that the partial solution of (2.36) which tends to zero exponentially as  $n \rightarrow \pm\infty$  is the solitary wave solution

$$\exp(-b\rho_n) - 1 = \frac{\sinh^2 q}{\cosh^2 [q(n - s\tau)]}, \quad (2.37)$$

where  $s > 1$  is the velocity of the wave and the parameter  $q$  is determined from the dispersion equation

$$s = \frac{\sinh q}{q}. \quad (2.38)$$

The acoustic soliton (2.37) can have any supersonic velocity. It follows from (2.38) that the velocity  $s \rightarrow 1 + 0$  as  $q \rightarrow 0$  and  $s$  tends to infinity as  $q \rightarrow \infty$ . The parameter  $q$  determines the reciprocal width of the soliton.

It is easily shown that the displacement has the form [8]

$$u_n(\tau) = \frac{1}{b} \ln \left[ \frac{1 + \exp(-2q) \exp 2q(n - s\tau)}{1 + \exp 2q(n - s\tau)} \right] + \text{const.} \quad (2.39)$$

The relative displacement is

$$\rho_n = u_{n+1} - u_n = -\frac{1}{b} \ln \frac{1 + \sinh^2(q)}{\cosh^2 q(n - s\tau)} < 0 ,$$

whence the chain is compressed in a region of soliton localization. The total chain compression is

$$u_{-\infty} - u_{+\infty} = \frac{2q}{b} .$$

As a result of chain compression, there is an excess of mass in the chain that allows us to attribute a mass to the soliton (soliton mass  $m = 2q/b$  in dimensionless units). The energy of the soliton is

$$E = \sum_{n=-\infty}^{+\infty} \frac{1}{2} u_n'^2 + U(\rho_n) = \frac{2}{b^2} [\sinh(q) \cosh q - q] . \quad (2.40)$$

The profile of the acoustic soliton in the Toda chain is shown in Fig. 2.3 (left). In terms of absolute  $u_n$  or relative  $\rho_n$  displacements, the acoustic soliton is described, respectively, by the step function (Fig. 2.3a left) or the bell-shaped function, corresponding to chain compression (Fig. 2.3b left). When the soliton velocity increases, its width decreases and the amplitude grows. At all values  $s > 1$ , the solitons interact with each other as elastic particles. When they collide, they repel each other (see Fig. 2.3 right). Furthermore, the solitons exchange momentum as perfect rigid particles, the only difference being a minor delay that occurs during their repulsion [8].

The Toda potential (2.34) appropriately describes molecular interaction during compression of intermolecular bonds, but it is not suitable for describing bond expansion. As can be seen in Fig. 2.2a (right), the potential rises exponentially for negative deformation ( $\rho < 0$ ), and linearly for positive deformation ( $\rho > 0$ ). Hence, it is not generally used to model molecular chain dynamics.

The deformation of valence bonds is more frequently described by the Morse potential

$$U(\rho) = \varepsilon [\exp(-\beta\rho) - 1]^2 , \quad (2.41)$$

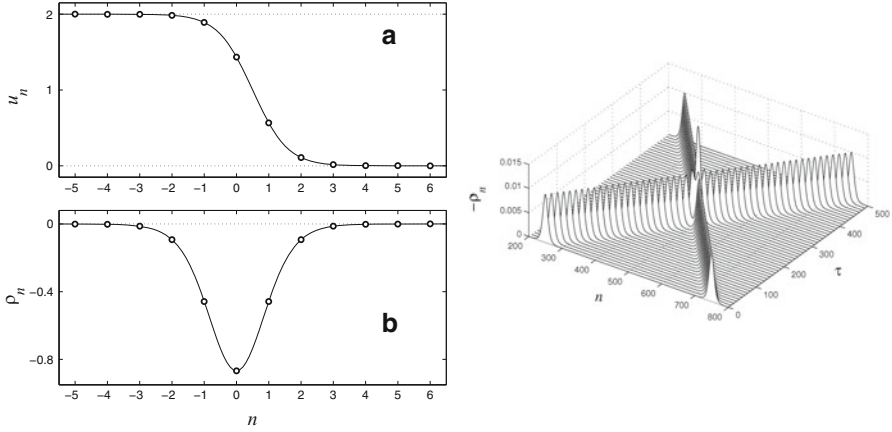


**Fig. 2.3** *Left:* Acoustic soliton in the Toda chain with  $b = 1$ ,  $q = 1$ , ( $s = 1.1752$ ). The distribution of the absolute  $u_n$  (a) and relative  $\rho_n$  (b) displacements of the links in the chain is shown. *Right:* Collision of the two acoustic solitons in the Toda chain with  $b = 1$ ,  $s = 1.017$  ( $q = 0.1$ ). The distribution of the relative chain displacements  $\rho_n$  is shown as a function of time  $\tau$

where the parameter  $\varepsilon$  corresponds to the bond energy and the parameter  $\beta$  describes the anharmonicity of the potential. The potential profile is shown in Fig. 2.2b (right). The potential grows exponentially as  $\varepsilon \exp(-2\beta\rho)$  when  $\rho \rightarrow -\infty$  and tends to  $\varepsilon$  when  $\rho \rightarrow +\infty$ .

The disadvantage of the Morse potential is that it allows the molecules to pass through each other since it is defined for all values of the displacements  $\rho$ . To prevent this, one must add a repulsive core to the potential. Given the equilibrium intermolecular bond length  $a$ , the energy of the potential must tend to infinity when the bond compression reaches the value  $a$ . The Lennard-Jones potential ( $2n, n$ ), being a potential with a repulsive core, is most frequently used:

$$U(\rho) = \varepsilon \left[ \left( 1 + \frac{\rho}{a} \right)^{-n} - 1 \right]^2, \quad (2.42)$$

where  $n = 1, 2, 3, \dots$ . At  $n = 6$ , the potential (2.42) describes the weak nonvalence van der Waals interaction of molecules with reasonable accuracy. The potential profile is shown in Fig. 2.2c (right). It is defined only for the relative displacement  $\rho > -a$ . The potential tends to  $U(\rho) \rightarrow +\infty$  as  $\rho \rightarrow -a$  and  $U(\rho) \rightarrow \varepsilon$  as  $\rho \rightarrow +\infty$ .

In contrast to the Toda chain, a chain with the Morse interaction potential (2.41) or the Lennard-Jones potential (2.42) is not a completely integrable system. Nevertheless, there exist acoustic solitons in these systems at all supersonic values of the velocity, although some peculiarities manifest themselves in the dynamics. As the Lennard-Jones potential differs most significantly from the Toda potential, the peculiarities must be more pronounced in this case. The profile of the soliton

(solitary wave) in the Morse and Lennard-Jones chains can only be obtained numerically.

## 2.4 Numerical Methods for Finding Soliton Solution

A solitary wave can be found in a discrete chain with a high degree of accuracy using the Eilbeck–Flesh pseudospectral method [6, 7]. In terms of the absolute displacement  $u_n$ , the chain dynamics is described by infinite-dimensional systems of discrete equations (2.13). In terms of the relative displacement  $\rho_n = u_{n+1} - u_n$ , the equations of motion have the form

$$\rho_n'' = F(\rho_{n+1}) - 2F(\rho_n) + F(\rho_{n-1}), \quad n = 0, \pm 1, \pm 2, \dots \quad (2.43)$$

Let us search for a solution of this system as a solitary wave of unchanged profile which moves with constant velocity  $s$ :  $\rho_n(s) = \rho(n - s\tau) = \rho(z)$ , where  $z = n - s\tau$  is the continuum wave variable  $z = n - s\tau$ . The wave profile  $\rho(z) \rightarrow 0$  and its derivative  $\rho'(z) \rightarrow 0$  as  $z \rightarrow \infty$ .

Replacing the discrete variable  $n$  by a continuous one  $z$ , (2.43) takes the form

$$s^2 \frac{d^2 \rho}{dz^2} \Big|_{z=n} = F(\rho(n+1)) - 2F(\rho(n)) + F(\rho(n-1)), \quad n = 0, \pm 1, \pm 2, \dots \quad (2.44)$$

The main idea of this method is to approximate the explicit soliton solution  $\rho(z)$  by the finite Fourier series on a finite interval  $-L/2 \leq z \leq L/2$ :

$$\rho(z) \approx R(z) = \sum_{k=0}^K a_k c_k(z), \quad (2.45)$$

where  $c_k(z) = \cos(2\pi k z / L)$ ,  $k = 0, 1, 2, \dots, K$ . Substituting (2.45) into (2.44) leads to the continuous equation

$$\mathcal{F}(z) = s^2 \sum_{k=0}^K a_k \left( \frac{2\pi k}{L} \right)^2 c_k(z) + G(z+1) - 2G(z) + G(z-1) = 0, \quad (2.46)$$

where

$$G(z) = F\left(\sum_{k=0}^K a_k c_k(z)\right).$$

The Fourier coefficients  $\{a_k\}_{k=0}^K$  can be found numerically as the roots of the system of  $K$  nonlinear equations

$$\begin{aligned} \rho(L/2) &= \sum_{k=0}^K a_k c_k(L/2) = 0, \\ \mathcal{F}(z_i) &= 0, \quad i = 0, 1, \dots, K-1, \end{aligned} \quad (2.47)$$

where  $z_i = iL/2K$  and the function  $\mathcal{F}(z)$  is given by (2.46).

This method can unambiguously answer the question about the existence of a soliton for any value of the velocity  $s$ . The absence of a soliton solution of (2.47) implies the impossibility of soliton motion for a given value of  $s$ . When solving (2.47) numerically, it suffices to put  $K = 100$  and  $L = 10D$ , where  $D$  is the diameter of the soliton solution given by

$$D = 2 \left[ \frac{\int_0^{L/2} z^2 \rho(z) dz}{\int_0^{L/2} \rho(z) dz} \right]^{1/2}.$$

The value  $A = -\rho(0)$  describes the amplitude of the soliton (the maximum relative displacement of a chain link in a region of soliton localization). The soliton energy is

$$E = \sum_{n=-N_L}^{N_L} \frac{1}{2} v_n^2 + V(r(n)),$$

where  $N_L$  is an integer part of  $L/2$  and the velocity is

$$v_{-N_L-1} = 0, \quad v_{n+1} = v_n + s \sum_{k=1}^K \frac{2\pi k a_k}{L} \sin \frac{2\pi k n}{L}, \quad n = -N_L, -N_L + 1, \dots, N_L.$$

## 2.5 Solitons in the Lennard-Jones Chain

Here we consider a chain with the Lennard-Jones potential (12,6) and parameters  $a = 1$  and  $\varepsilon = 1/72$ . Note that, at these parameter values, the potential rigidity is  $U''(0) = 72\varepsilon/a^2 = 1$ . Numerical solution of (2.47) has shown that acoustic solitons exist in the chain at all supersonic values of the velocity  $s > 1$ . The dependencies of the soliton amplitude  $A$ , diameter  $D$ , and energy  $E$ , on the velocity  $s$ , are shown in Fig. 2.4 (left). As can be seen from Fig. 2.4a and b (left), the amplitude  $A$  tends

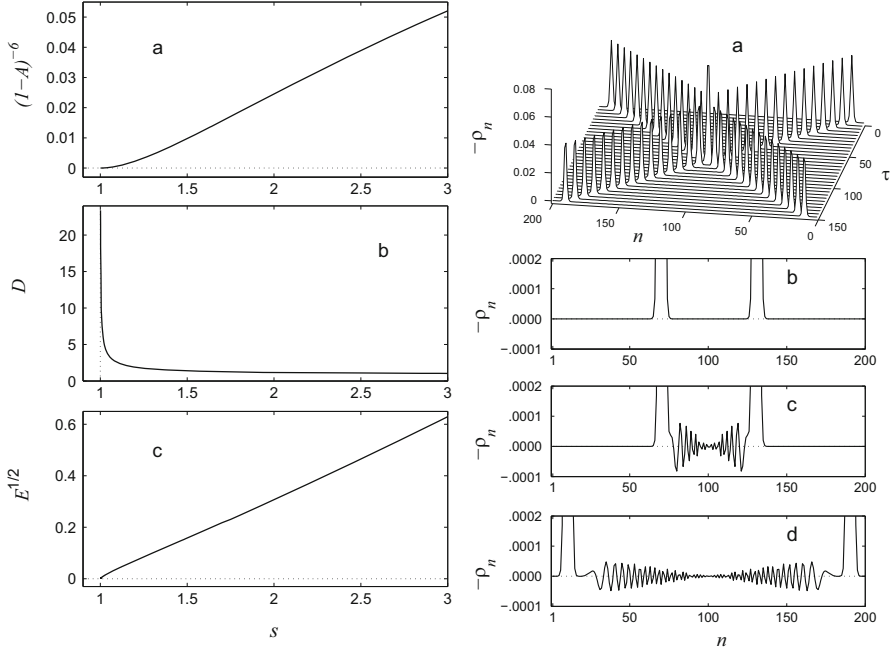


**Fig. 2.4** *Left:* Dependence of the function  $(1 - A)^{-6}$  of the amplitude  $A$  (a), the width  $D$  (b), and the square root of the energy  $\sqrt{E}$  (c) on the velocity of the acoustic soliton  $s$  in the Lennard-Jones chain. *Right:* Collision of acoustic solitons in the Lennard-Jones chain at velocity  $s = 1.2$  (a). The soliton profile before the collision at time  $\tau = 50$  (b) and after collision at  $\tau = 100$  (c) and  $\tau = 150$  (d)

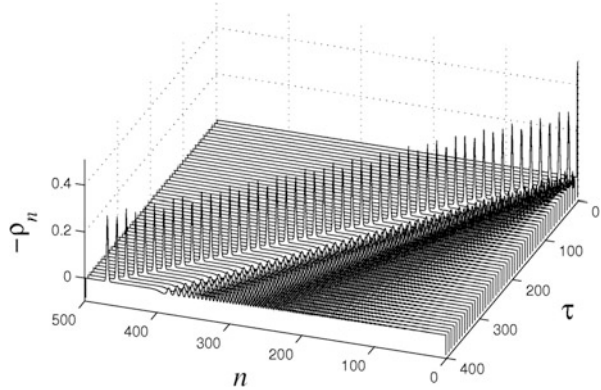
steadily to 1 as  $1 - O(s^{-1/6})$ , while the soliton diameter  $D$  decreases monotonically. The soliton width becomes less than 10 at  $s = 1.0055$ , 5 at  $s = 1.0226$ , 2 at  $s = 1.175$ , and finally less than 1 at  $s = 3.7$ , at which point it is less than the chain spacing. The soliton energy increases steadily as  $s^2$  (see Fig. 2.4b left).

As the Lennard-Jones chain is not a completely integrable system, the soliton interaction is no longer elastic. The collision of two solitons is accompanied by the emission of low-amplitude waves (phonons). The non-elasticity of the soliton interaction can be characterized by the energy loss  $p = [(E_1 - E_2)/E_1]100\%$ , where  $E_1$  and  $E_2$  are the soliton energies before and after collision, respectively. The dependence of the energy loss  $p$  on the velocity  $s$  is given in Table 2.1. The maximum energy loss  $p = 0.00083\%$  is observed for  $s = 1.23$ . The soliton collision is shown in Fig. 2.4 (right). The phonon emission can be observed only at a high magnification. Therefore, the weak ‘non-elasticity’ of the soliton interaction is related to the proximity of the Lennard-Jones chain to a completely integrable system. The energy loss at the collision tends to zero as  $s \rightarrow 1 + 0$  (in this limit, the soliton dynamics is described by the continuous integrable Boussinesq equation)



**Table 2.1** Dependence of the energy loss (%) in a soliton collision in the Lennard-Jones chain on their velocity  $s$ 

$s$	1.03	1.06	1.1	1.2	1.23
$p$ (%)	$1.4 \times 10^{-5}$	$1.1 \times 10^{-4}$	$3.7 \times 10^{-4}$	$8.1 \times 10^{-4}$	$8.3 \times 10^{-4}$
$s$	1.3	2.0	2.5	3.0	3.5
$p$ (%)	$7.6 \times 10^{-4}$	$5.6 \times 10^{-5}$	$7.9 \times 10^{-6}$	$9.8 \times 10^{-7}$	$4.6 \times 10^{-8}$

**Fig. 2.5** Formation of the acoustic soliton in the chain with the Morse potential ( $\varepsilon = 0.5$ ,  $\beta = 1$ ) as a result of the compression of the first bond in the molecular chain of  $N = 500$  molecules. Dependence of the distribution of the local displacement  $\rho_n$  in the chain on the time  $\tau$ 

and as  $s \rightarrow \infty$  (where the dynamics is described by an integrable system of rigid spheres).

Thus, the acoustic solitons in the Lennard-Jones chain exist at all supersonic values of the velocity  $s > 1$ . The solitons interact virtually as rigid particles. The maximum soliton energy loss observed at collision for  $s = 1.23$  is only 0.00083 % of their energy. The solitons in the chain with the Morse interaction potential can be considered to be interacting elastically.

The acoustic solitons are formed as a result of the compression of molecular bonds. To model the formation of the soliton, it is best to consider a finite chain of  $N$  molecules, subjected to the compression of its end link by a value  $\rho_0 > 0$  at the initial moment of time. The chain dynamics will be described by the equations

$$u_n'' = F(u_{n+1} - u_n) - F(u_n - u_{n-1}), \quad n = 2, 3, \dots, N-1, \quad u_1 \equiv \rho_0, \quad u_N \equiv 0, \quad (2.48)$$

with initial conditions  $u_n(0) = 0$  and  $u_n'(0) = 0$ . Let us take here the Morse potential (2.41) with parameters  $\varepsilon = 0.5$ ,  $\beta = 1$ . For these parameters, the potential rigidity  $U''(0) = 1$ . Numerical simulation of the soliton dynamics shows that the compression of a single finite link leads to the formation of an acoustic soliton in the chain, along with a spreading wave packet moving with the velocity of sound (see Fig. 2.5). The bigger the initial compression of the link, the bigger fraction of the energy accumulated by the soliton. The fraction of the soliton energy relative to the total energy is  $p = 0.504$  for  $\rho_0 = 0.1$ ,  $p = 0.718$  for  $\rho_0 = 0.2$ , and  $p = 0.922$  for

$\rho_0 = 0.5$ . Thus, in the anharmonic chain, the energy of the dynamic compression of the chain end is effectively transferred along the chain by the acoustic soliton.

## 2.6 Solitons in the Diatomic Chain

The diatomic chain with nonlinear intermolecular interaction has become a subject of close attention in connection with modeling thermal conductivity in nonmetallic crystals [14–16]. Anomalies in the thermal conductivity of nonlinear systems were first observed in the notable work of Fermi, Pasta, and Ulam [1]. It has been realized by now that the impact of nonlinearity, in the context of the classical theory of thermal conductivity, does not reduce to the inelastic phonon–phonon interaction. Experimentally observed thermal solitons in the quasi-one-dimensional system [17] can significantly modify the character of thermal conductivity. Moreover, no one has yet succeeded in deriving the thermal conductivity equation from first principles.

The diatomic Toda lattice has the property of complete integrability in the case of equal masses [8] and exhibits stochastic behavior for a specific mass ratio [15]. To understand the features of the dynamical behavior of this system and the mechanism underlying its thermal conductivity, one must determine the dynamical properties of the acoustic solitons. We thus investigate numerically the soliton dynamics in the diatomic Toda lattice. We will show that the soliton motion in a given system is always accompanied by a phonon emission which is insignificantly small in the range of the sound velocity and steadily increases when the soliton velocity increases.

### 2.6.1 Model of the Diatomic Chain

Consider a chain consisting of particles of masses  $m_1$  and  $m_2$ , which are located at a fixed interval  $a$  from each other. The model is shown schematically in Fig. 2.6. We describe the interaction of the neighboring particles by the Toda potential

$$V(\rho) = Kb^{-1} \left\{ \rho + b^{-1} [\exp(-b\rho) - 1] \right\},$$

where  $\rho$  is the relative change in the intermolecular distance,  $K$  is the rigidity coefficient, and  $b$  is the potential anharmonicity parameter.

The Hamiltonian of the system can be represented in the form

$$H = \sum_n \left[ \frac{1}{2} m_1 \dot{x}_{2n}^2 + \frac{1}{2} m_2 \dot{x}_{2n+1}^2 + V(\rho_{2n}) + V(\rho_{2n+1}) \right], \quad (2.49)$$

where the dot denotes differentiation with respect to time  $t$ ,  $x_n$  is the displacement of the  $n$ th site from its equilibrium position, and  $\rho_n = x_{n+1} - x_n$  is the relative

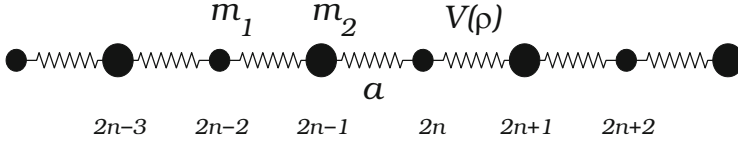


**Fig. 2.6** Schematic view of the diatomic molecular chain

displacement of the  $n$ th site. The following equations of motion correspond to the Hamiltonian (2.49):

$$m_1 \ddot{x}_{2n} = F(\rho_{2n}) - F(\rho_{2n-1}), \quad m_2 \ddot{x}_{2n+1} = F(\rho_{2n+1}) - F(\rho_{2n}), \quad n = 0, \pm 1, \pm 2, \dots, \quad (2.50)$$

where  $F(\rho) = dV/d\rho$ . For small-amplitude waves, the dispersion equation is readily found to be

$$\omega^4 m_1 m_2 - 2K(m_1 + m_2)\omega^2 + 4K^2 \sin^2(\lambda a) = 0,$$

where  $\omega$  is the wave frequency and  $0 \leq \lambda \leq \pi/a$  is the wavenumber. This gives the velocity of sound in the form (the velocity of long-wavelength, small-amplitude waves)

$$v_0 = \lim_{\lambda \rightarrow 0} \frac{\omega(\lambda)}{\lambda} = a \sqrt{2K/M},$$

where the mass  $M = m_1 + m_2$ .

For the convenience of calculation, we introduce the dimensionless displacement  $u_n = x_n/a$ , time  $\tau = t \sqrt{2K/M}$ , and energy  $\mathcal{H} = H/Ka^2$ . Then the Hamiltonian of the chain (2.49) takes the form

$$\mathcal{H} = \sum_n \left[ \frac{1}{2} \mu_1 u_{2n}'^2 + \frac{1}{2} \mu_2 u_{2n+1}'^2 + U(r_{2n}) + U(r_{2n+1}) \right],$$

where the prime denotes differentiation with respect to time  $\tau$ ,  $\mu_i = 2m_i/M$ ,  $i = 1, 2$ , is the dimensionless mass,  $r_n = u_{n+1} - u_n$  is the relative displacement, and the potential is

$$U(r) = \beta^{-1} \left\{ r + \beta^{-1} [\exp(-\beta r) - 1] \right\}, \quad (2.51)$$

with  $\beta = ab$ . In terms of the dimensionless variables, the equations of motion (2.50) take the form

$$\mu_1 u''_{2n} = G(r_{2n}) - G(r_{2n-1}), \quad \mu_2 u''_{2n+1} = G(r_{2n+1}) - G(r_{2n}), \quad n = 0, \pm 1, \pm 2, \dots, \quad (2.52)$$

where  $G(r) = dU/dr = \beta^{-1}[1 - \exp(-\beta r)]$ .

### 2.6.2 Continuum Approximation

Hereafter, for simplicity, we shall put  $\beta = 1$ . Then the dimensionless Toda potential (2.51) for the small-amplitude displacements has the form

$$U(r) \approx \frac{1}{2}r^2 - \frac{1}{6}r^3.$$

Let us use the continuum approximation  $u_n(\tau) = u(x, \tau)|_{x=n}$ . Then the equations of motion (2.52) lead to the well-known Boussinesq equation [18, 19]:

$$u_{\tau\tau} = u_{xx} - u_x u_{xx} + \frac{1}{12} c u_{xxxx}. \quad (2.53)$$

We will search for its solution in the form of a wave of constant shape  $u_n(\tau) = u(\xi)$ , where  $\xi = n - s\tau$  is the wave variable and  $s > 1$  is the wave velocity.

As a result of the series of elementary approximations, (2.53) leads to the following equation in terms of the relative displacement  $r = u_\xi$ :

$$(1 - s^2)r^2 - \frac{1}{3}r^3 + \frac{1}{3}cr_\xi^2 = 0,$$

where the coefficient  $c = 1 - 3\mu_1\mu_2/4$ . The solution of this equation has the form

$$r(\xi) = -\frac{A}{\cosh^2(\alpha\xi)}, \quad (2.54)$$

where  $A = 3(s^2 - 1)$  and  $\alpha = \sqrt{3(s^2 - 1)/4c}$  are the amplitude and the reciprocal width of the soliton, respectively.

### 2.6.3 Numerical Simulation of Soliton Dynamics

Let us consider the dynamics of an acoustic soliton in a chain with  $\mu_1 = \mu$  and  $\mu_2 = 2 - \mu$ , where  $0 < \mu \leq 1$ . We numerically integrated the equations of motion (2.52) with  $n = 1, \dots, N$ ,  $N = 300$  and boundary conditions ( $u'_1 \equiv 0$ ,  $u_N \equiv 0$ ) at the fixed ends. The soliton solution (2.54) was taken as the initial condition.

Let the center of the soliton be located at the site  $n = N/2$  at the initial time. To model the soliton dynamics in an infinite chain, we shift the soliton back just as it passes 100 links of the chain, i.e., we carry out the substitution

$$\begin{aligned} u_n(\tau) &= u_{n+100}, \quad n = 1, \dots, N-100, \quad u_n(\tau) = 0, \quad n = N-99, \dots, N \\ u'_n(\tau) &= u'_{n+100}, \quad n = 1, \dots, N-100, \quad u'_n(\tau) = 0, \quad n = N-99, \dots, N. \end{aligned}$$

At each such point in time, the soliton is described by the current velocity  $s = 100/\tau_1$ , where  $\tau_1$  is the time of the soliton passage over 100 links and the energy is

$$E = \sum_{n=1}^{N/2-1} \left[ \frac{1}{2} \mu_1 u_{2n}^2 + \frac{1}{2} \mu_2 u_{2n+1}^2 + U(r_{2n}) + U(r_{2n+1}) \right].$$

The numerical integration showed that the soliton dynamics depends significantly on the ratio of particle masses  $\kappa = \mu_1/\mu_2$ . For  $\kappa = 1$  ( $\mu_1 = \mu_2 = 1$ ) and  $\kappa = 0$  ( $\mu_1 = 0, \mu_2 = 2$ ), the equations of motion become completely integrable. Therefore, the soliton motion occurs without phonon emission. The soliton moves with a constant velocity. However, the intermediate value of  $\kappa$  is more interesting. In the intermediate region, the soliton motion is always accompanied by phonon emission (see Fig. 2.7 left), leading to the slowing down of the soliton. This phenomenon is conveniently described by the fraction of its energy which is lost

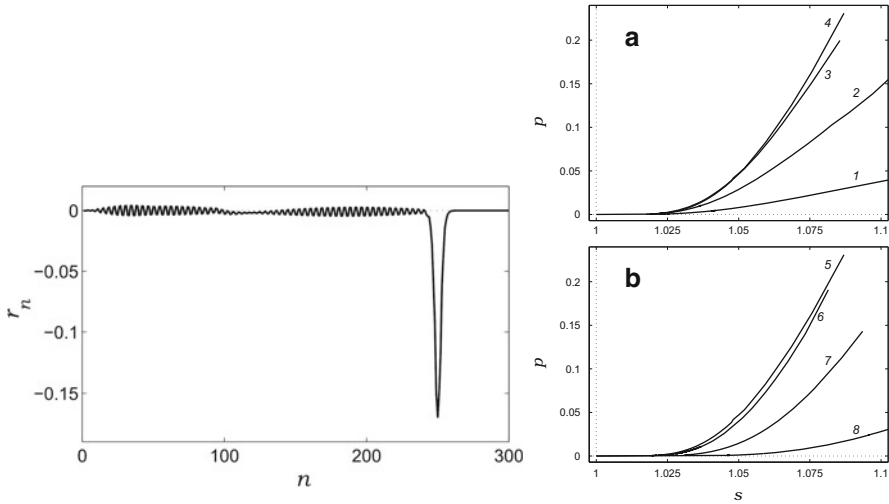
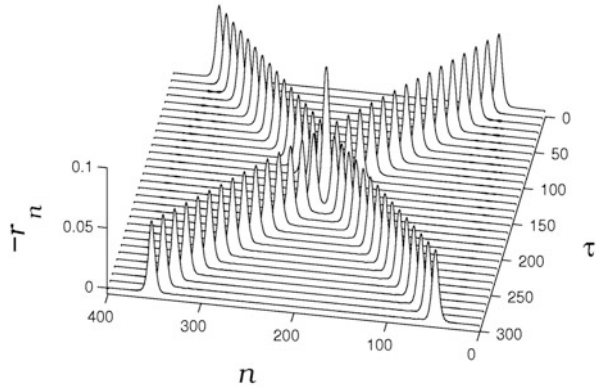


**Fig. 2.7** *Left*: Phonon emission of the acoustic soliton in the diatomic chain. Soliton velocity  $s = 1.03$  and mass ratio  $\kappa = 0.65$ . *Right*: Dependence of the soliton energy loss  $p$  on the velocity  $s$  at (a)  $\kappa = 0.9, 0.8, 0.7$ , and  $0.65$  (lines 1, 2, 3, and 4, respectively) and (b)  $\kappa = 0.65, 0.6, 0.5$ , and  $0.4$  (lines 5, 6, 7, and 8, respectively)

**Fig. 2.8** Elastic collision of acoustic solitons in the diatomic chain ( $\kappa = 0.65$ ) at the velocity  $s = 1.01$



when it passes 100 links of the chain:

$$p(\tau) = \frac{E(\tau) - E(\tau + \tau_1)}{E(\tau)}.$$

The dependence of the soliton energy loss  $p$  on its velocity  $s$  is shown in Fig. 2.7 (right) for different values of  $\kappa$ . As can be seen, when the velocity decreases, the energy loss decreases proportionally to  $(1 - s)^2$ . The value of the proportionality coefficient depends on  $\kappa$ . With  $\kappa$  decreasing from 1 to 0.65, the energy loss grows steadily. The maximal loss is observed at  $\kappa = 0.65$ . A further decrease in  $\kappa$  no longer leads to a monotonic decrease in the energy loss (see Fig. 2.7 right).

For velocities with  $1 < s < 1.015$ , phonon emission by the soliton becomes negligibly small. In this case the solitons actually move with constant velocities and interact as rigid particles (see Fig. 2.8).

The modeling performed here has shown that, in the diatomic chain, acoustic soliton motion is always accompanied by phonon emission. The emission is negligibly small in the range of the sound speed ( $1 < s < 1.015$ ), but as the soliton velocity increases, the fraction of the energy emitted by the phonons grows proportionally to  $(1 - s)^2$ . These results allow us to conclude that the equipartition of energy in diatomic chains happens as a result of the intensive emission of phonons by the acoustic solitons. Maximal emission is reached at the ratio of particle masses of the chain  $\kappa = m_1/m_2 = 0.65$ . It is for this value of  $\kappa$  that the effect of chaos in the system dynamics is expected to be the most pronounced.

## 2.7 Acoustic Solitons in a Helix Chain

The development of modern nonlinear physics has led to the discovery of new elementary mechanisms which determine the behavior of many physical processes in crystals and other ordered molecular systems at the molecular level. Today,

the role of acoustic solitons, ensuring the most efficient mechanisms of energy transfer in such processes as heat conductivity, fracture of solids [20–23], and signal propagation in biological macromolecules, is quite clear [24].

One pioneering theoretical study of the nonlinear dynamics of macromolecular chains [1, 4, 12, 25] considered the one-dimensional (spatial-linear) models with positive anharmonicity, in which only the longitudinal displacements of atoms (molecules) in the chain were taken into account. In this case, when neighboring sites of a chain approach each other, the repulsive force between them increases faster than in the harmonic approximation. One of the consequences of this is the existence of dynamically stable solitary waves of compression which are referred to as supersonic acoustic solitons.

Essentially, acoustic solitons do not interact with longitudinal acoustic phonons, so they transfer energy in a loss-free manner over long distances. The process changes dramatically if the transverse and longitudinal displacements are taken into account. In this case, the soliton will have a finite path length and its motion will be accompanied by emission of transverse and orientational phonons of the chain.

The effect of the transverse molecular oscillations in a chain on the soliton dynamics was considered for the first time in [26]. Solitons turned out to be highly sensitive to longitudinal perturbations. This problem was investigated comprehensively in [27–32]. The soliton interaction with orientational molecular oscillations was analysed in [33].

For a series of biomolecular chains, it is hard to understand the way they function without considering the transverse motion of the chain links. Thus, in the DNA molecule, the stretching of base pairs in the transverse direction makes denaturation possible. The Peyrard–Bishop model of DNA melting [34–36] considered only the transverse motion of complimentary base pairs. Although the DNA molecule (having both longitudinal and transverse degrees of freedom) is considered as an isolated object, this model actually describes the one-dimensional dynamics of the molecular chain in an effective substrate potential. A comprehensive review of models of DNA nonlinear dynamics is given in [37].

The geometric structure of biomolecular systems requires use of two- and three-dimensional models. This is the only way to take into account the system's anharmonicity, which is determined by its molecular geometry. For example, in the framework of the simplest cluster model of the  $\alpha$ -chymotrypsin enzyme, it was shown that geometric anharmonicity in the two-dimensional system makes energy transfer between degrees of freedom possible, even for small amplitudes [38, 39].

Applying current computational power to the analysis of nonlinear molecular systems dynamics, one can move from simple one-dimensional models to more complex two- and three-dimensional models, which take into account the geometrical structure of the system in a realistic way. The simplest and most convenient objects from this point of view are the zigzag molecular chains for which the nonlinear dynamics is considered in detail in [40–44]. To understand the mechanisms at work in the majority of biological systems, a two-dimensional model is inappropriate. The simplest example of such a system is a protein  $\alpha$ -helix macromolecule.

Consider the three-dimensional dynamics of a free molecular chain. Clearly, the chain, in the absence of a substrate, will have a ground state with a regular stable structure only if the interaction between the remote neighbours is taken into account in addition to the short-range interaction. The inclusion of the long-range interaction results in the appearance of a *secondary structure*, of the chain, which is often encountered in many macromolecules (DNA, proteins, and the like). Geometrically, the secondary structure is realized in the form a helix.

The three-dimensional dynamics of a helix chain was analysed in [45], where the existence of the three-dimensional acoustic soliton of compression was shown. The existence of this soliton is associated with the physical anharmonicity (anharmonicity of intermolecular interaction).

Here we consider in detail the soliton dynamics in the helix chain. We will show that, along with a soliton of longitudinal compression, there also exists another type of soliton in the helix, namely the soliton of torsion. In this case, the existence of this soliton is associated with the geometrical anharmonicity of the helix. This anharmonicity is determined by three-dimensional structure of the helix and manifests itself even if all the intermolecular interaction forces are harmonic. The geometrical anharmonicity was first studied in [46], where it was shown that this anharmonicity can ensure the existence of a breather-like excitation in a linear molecular chain.

### 2.7.1 Model of a Helix Chain

Consider a molecular helix chain shown in Fig. 2.9 (left), in which each molecule (peptide group) of the chain interacts with its six nearest neighbors. The interaction between first neighbors is the strongest. It is mainly due to the deformation of the rigid valence bonds. The interaction between second neighbors results from the deformation of the softer valence angles. The interaction between third neighbors is the weakest. It is described by the non-valence molecular interaction. These three types of interaction stabilize the three-dimensional helix chain, provided that each molecule of the chain can move in three  $(x, y, z)$  directions.

The geometry of the helix chain is uniquely given by a set of three parameters: the radius  $R_0$ , the angular spacing  $\phi$ , and the longitudinal spacing  $\Delta z$  of the helix. In the equilibrium position, the radius vector of the  $n$ th site of the helix is

$$\mathbf{R}_n = R_0(\cos(n\phi), \sin(n\phi), nh), \quad n = 0, \pm 1, \dots,$$

where  $h = \Delta z/R_0$  is the dimensionless longitudinal spacing of the helix. The angular spacing of the helix satisfies  $|\phi| \leq \pi$ . The helix is right-handed for  $\phi > 0$  and left-handed for  $\phi < 0$ . When  $\phi = \pm\pi$ , the three-dimensional helix degenerates into a planar zigzag structure.

The helix can also be uniquely specified by the distances between three neighboring molecules, i.e., the distances  $D_1$ ,  $D_2$ , and  $D_3$  between the first, second, and



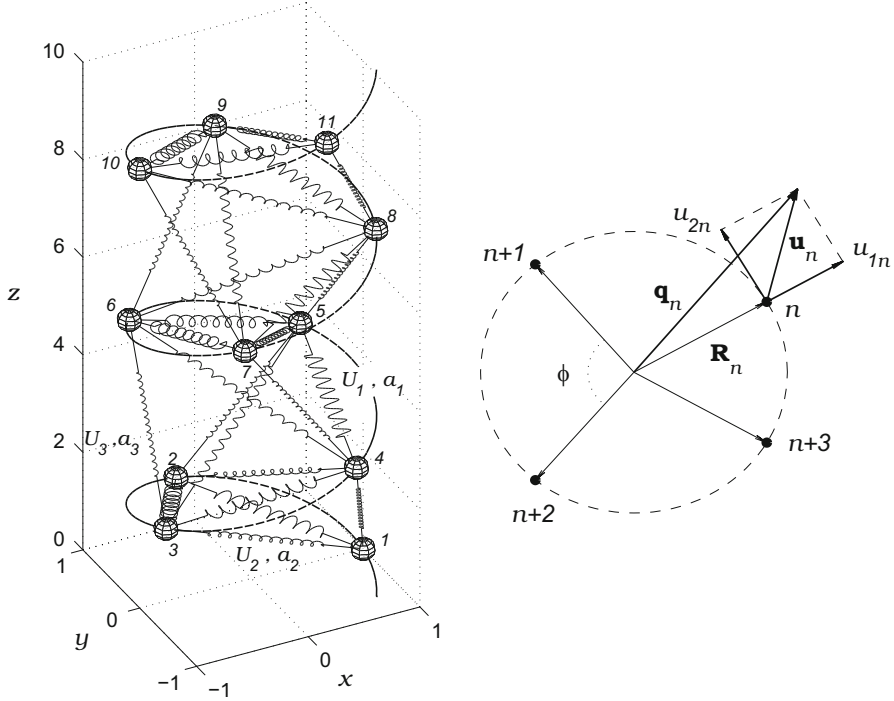


**Fig. 2.9** *Left*: Fragment of the helix chain consisting of 11 molecules. The geometry of the chain corresponds to an  $\alpha$ -helix ( $\phi = 100^\circ$ ). The intermolecular potentials  $U_j$ ,  $j = 1, 2, 3$  are shown schematically by the springs of different diameters (spring thickness corresponds to interaction rigidity). *Right*: Local coordinate system in the  $xy$  plane

third neighbors. The dimensionless nearest-neighbor intermolecular distance is

$$a_j = \frac{D_j}{R_0} = \sqrt{2[1 - \cos(j\phi)] + j^2 h^2}, \quad j = 1, 2, 3. \quad (2.55)$$

It follows from (2.55) that the angular spacing  $\phi$  of the helix obeys

$$\frac{3 - 4 \cos \phi + \cos(2\phi)}{8 - 9 \cos \phi + \cos(3\phi)} = \frac{4a_1^2 - a_2^2}{9a_1^2 - a_3^2}. \quad (2.56)$$

After solving (2.56), we readily obtain

$$R_0 = \frac{\sqrt{4D_1^2 - D_2^2}}{4 \sin^2(\phi/2)}, \quad \Delta z = \frac{\sqrt{D_2^2/4 - D_1^2 \cos^2(\phi/2)}}{\sin(\phi/2)}.$$

The Hamiltonian of the helix chain has the form

$$H = \sum_n \left[ \frac{1}{2} M (\dot{x}_n^2 + \dot{y}_n^2 + \dot{z}_n^2) + K R_0^2 \sum_{j=1,2,3} U_j(r_{jn}) \right], \quad (2.57)$$

where  $M$  is the mass of a single link of the chain, and  $x_n$ ,  $y_n$ , and  $z_n$  are the displacements of the  $n$ th chain link from its equilibrium position. The dot denotes differentiation with respect to time  $t$ . The constant  $K$  defines the rigidity of intermolecular interaction. The dimensionless potential  $U_j(r_{jn})$  describes the interaction between the  $n$ th and the  $(n+j)$ th molecules, and  $r_{jn} = R_{jn}/R_0$  is the dimensionless distance between them. The interaction potentials are normalized by the conditions  $U_j(a_j) = 0$ ,  $U'_j(a_j) = 0$ ,  $j = 1, 2, 3$ .

We describe the molecular interaction by the Morse potentials

$$\begin{aligned} U_j(r) &= \frac{1}{2} \frac{\kappa_j}{\gamma_j^2} \left\{ 1 - \exp[-\gamma_j(r - a_j)] \right\}^2 \\ &= \frac{1}{2} \kappa_j (r - a_j)^2 [1 - \gamma_j(r - a_j) + \dots], \quad j = 1, 2, 3, \end{aligned} \quad (2.58)$$

where  $\kappa_j = K_j/K = U''_j(a_j)$  is the dimensionless rigidity of the interaction and  $\gamma_j$  is the anharmonicity parameter. In the limit  $\gamma_j \rightarrow 0$ , the potential (2.58) turns into the harmonic potential

$$U_j(r) = \frac{1}{2} \kappa_j (r - a_j)^2, \quad j = 1, 2, 3.$$

For further calculation, it is convenient to introduce the dimensionless time

$$\tau = \omega_0 t, \quad \omega_0 = \sqrt{K/M},$$

and dimensionless displacement vectors

$$\mathbf{q}_n = (q_{1n}, q_{2n}, q_{3n}) = \frac{\mathbf{R}_n}{R_0} + \mathbf{v}_n, \quad \mathbf{v}_n = (v_{1n}, v_{2n}, v_{3n}) = \frac{1}{R_0} (x_n, y_n, z_n). \quad (2.59)$$

Then the dimensionless distances  $r_{jn} = |\mathbf{q}_{n+j} - \mathbf{q}_n|$  and the Hamiltonian of the chain (2.57) can be rewritten in the dimensionless form

$$\mathcal{H} = \frac{H}{K R_0^2} = \sum_n \left[ \frac{1}{2} \left( \frac{d\mathbf{q}_n}{d\tau} \right)^2 + \sum_{j=1,2,3} U_j(|\mathbf{q}_{n+j} - \mathbf{q}_n|) \right]. \quad (2.60)$$

The equations of motion corresponding to the Hamiltonian (2.60) take the form

$$\frac{d^2 \mathbf{q}_n}{d\tau^2} = \sum_{j=1,2,3} \left[ W_j(r_{jn})(\mathbf{q}_{n+j} - \mathbf{q}_n) - W_j(r_{j,n-j})(\mathbf{q}_n - \mathbf{q}_{n-j}) \right],$$

$$n = 0, \pm 1, \pm 2, \dots, \quad (2.61)$$

where  $W_j(r_{jn}) = U'_j(r_{jn})/r_{jn}$ .

### 2.7.2 Dispersion Equation

It is more reasonable to consider the relative molecular displacement with respect to the equilibrium position locally for each molecule. For the equilibrium position of the  $n$ th molecule, we consider the coordinate system formed by the normal and the tangent to the circle  $z/R_0 = nh$ ,  $|\mathbf{q}| = 1$  in the  $xy$  plane, as shown in Fig. 2.9 (right). We denote the displacement vector  $\mathbf{v}_n$  in this coordinate system by  $\mathbf{u}_n = (u_{1n}, u_{2n}, u_{3n})$ , where  $u_{1n}$  and  $u_{2n}$  are the normal and tangential projections of the displacement vector, respectively, and  $u_{3n} = v_{3n}$  is the longitudinal coordinate. The new local coordinate system can be obtained by a rotational transformation, specified by

$$\mathbf{T}_n \mathbf{v}_n = \mathbf{u}_n, \quad \mathbf{T}_n = \begin{pmatrix} \cos(n\phi) & \sin(n\phi) & 0 \\ -\sin(n\phi) & \cos(n\phi) & 0 \\ 0 & 0 & 1 \end{pmatrix}. \quad (2.62)$$

The orthogonal operators  $\mathbf{T}_n$  form a group:  $\mathbf{T}_m \mathbf{T}_n = \mathbf{T}_{m+n}$ , where  $\mathbf{T}_0 = \mathbf{I}$  is the identity operator.

Substituting the expression  $\mathbf{q}_n = \mathbf{R}_n/R_0 + \mathbf{T}_n^{-1} \mathbf{u}_n$  (see (2.59) and (2.62)) into the equations of motion (2.61) yields

$$\frac{d^2 \mathbf{u}_n}{d\tau^2} = \sum_{j=1,2,3} \left[ \mathbf{T}_j^{-1} \mathbf{F}_j(\mathbf{u}_n, \mathbf{u}_{n+j}) - \mathbf{F}_j(\mathbf{u}_{n-j}, \mathbf{u}_n) \right], \quad n = 0, \pm 1, \pm 2, \dots,$$

where the intermolecular forces are defined by

$$\mathbf{F}_j(\mathbf{u}_n, \mathbf{u}_{n+j}) = W_j(r_{jn})(\mathbf{c}_j + \mathbf{u}_{n+j} - \mathbf{T}_j \mathbf{u}_n). \quad (2.63)$$

Here, the distance  $r_{jn}$  between the  $n$ th and the  $(n+j)$ th molecules is

$$\mathbf{r}_{jn} = |\mathbf{a}_{jn} + \mathbf{T}_{n+j}^{-1} \mathbf{u}_{n+j} - \mathbf{T}_n^{-1} \mathbf{u}_n|, \quad \mathbf{a}_{jn} = \frac{\mathbf{R}_{n+j} - \mathbf{R}_n}{R_0}, \quad (2.64)$$

and the constant vectors are defined by

$$\mathbf{c}_j = (1 - \cos(j\phi), \sin(j\phi), jh) . \quad (2.65)$$

As can be seen from (2.63)–(2.65), the right-hand side of the equations of motion (2.63) is not a function of the difference between the vectors  $\mathbf{u}_n$  and  $\mathbf{u}_{n+j}$ .

In the harmonic approximation ( $\gamma_j \rightarrow 0$ ,  $j = 1, 2, 3$ ), for all the intermolecular forces, we have

$$\mathbf{F}_j(\mathbf{u}_n, \mathbf{u}_{n+j}) = \alpha_j \langle (\mathbf{u}_{n+j} - \mathbf{T}_j \mathbf{u}_n), \mathbf{c}_j \rangle \mathbf{c}_j + \dots ,$$

where  $\alpha_j = \kappa_j / a_j^2$  and  $\langle \cdot, \cdot \rangle$  denotes the inner product. Substituting this expansion into (2.63) gives the linearized equations of motion:

$$\begin{aligned} \frac{d^2 \mathbf{u}_n}{d\tau^2} &= \sum_{j=1,2,3} \alpha_j \left[ \langle \mathbf{u}_{n+j} - \mathbf{T}_j \mathbf{u}_n, \mathbf{c}_j \rangle \mathbf{T}_j^{-1} \mathbf{c}_j - \langle \mathbf{u}_n - \mathbf{T}_j \mathbf{u}_{n-j}, \mathbf{c}_j \rangle \mathbf{c}_j \right] , \\ n &= 0, \pm 1, \pm 2, \dots \end{aligned} \quad (2.66)$$

Substituting the plane wave

$$\mathbf{u}_n = \mathbf{A}_n \exp[i(kn - \Omega\tau)]$$

into the linear equations (2.66), we obtain the following dispersion law:

$$\begin{vmatrix} \Omega^2 - c_{11} & -ic_{12} & -ic_{13} \\ ic_{12} & \Omega^2 - c_{22} & -c_{23} \\ ic_{13} & -c_{23} & \Omega^2 - c_{33} \end{vmatrix} = 0 , \quad (2.67)$$

where the coefficients are

$$\begin{aligned} c_{11} &= 2 \sum_j \alpha_j [1 - \cos(j\phi)]^2 [1 + \cos(jk)] , \\ c_{12} &= 2 \sum_j \alpha_j [1 - \cos(j\phi)] \sin(j\phi) \sin(jk) , \\ c_{13} &= 2 \sum_j \alpha_j jh [1 - \cos(j\phi)] \sin(jk) , \\ c_{22} &= 2 \sum_j \alpha_j \sin^2(j\phi) [1 - \cos(jk)] , \\ c_{23} &= 2 \sum_j \alpha_j jh \sin(j\phi) [1 - \cos(jk)] , \\ c_{33} &= 2 \sum_j \alpha_j j^2 h^2 [1 - \cos(jk)] . \end{aligned} \quad (2.68)$$

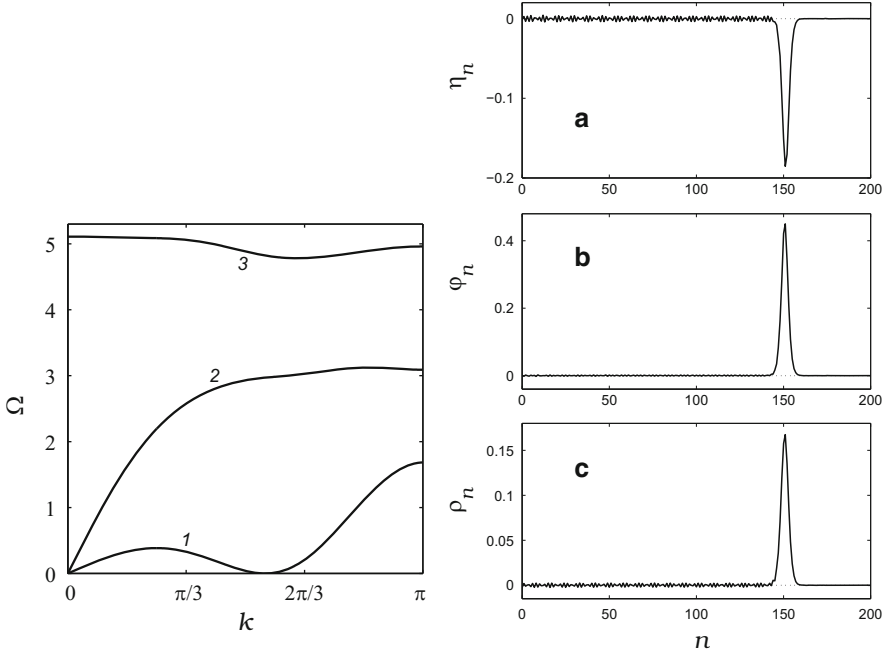


**Fig. 2.10** *Left:* Dependence of the frequencies  $\Omega_t$  (line 1),  $\Omega_l$  (line 2), and  $\Omega_{op}$  (line 3) on the wavenumber  $k$ ,  $0 \leq k \leq \pi$ . *Right:* The three-component profile of the torsion soliton at the velocity  $s = 1.5s_t$  ( $\gamma_3 = 0$ ). Phonon emission by the soliton is notable

More explicitly, the dispersion equation (2.67) has the form

$$\begin{aligned} \Omega^6 - (c_{11} + c_{22} + c_{33})\Omega^4 + (c_{11}c_{22} + c_{11}c_{33} + c_{22}c_{33} - c_{12}^2 - c_{13}^2 - c_{23}^2)\Omega^2 \\ + (c_{11}c_{23}^2 + c_{22}c_{13}^2 + c_{33}c_{12}^2 - c_{11}c_{22}c_{33} - 2c_{12}c_{13}c_{23}) = 0. \end{aligned} \quad (2.69)$$

Using the explicit form of (2.68) and (2.69), it can be shown that there are three non-degenerate, non-negative roots of the cubic equation (2.69) with respect to  $\Omega^2$  for  $0 < k \leq \pi$ . In the long-wavelength limit,  $k \rightarrow 0$ , the free term and the coefficient of  $\Omega^2$  in (2.69) tend to zero. Therefore, two of the three solutions of this equation correspond to the acoustic branches of the dispersion curve. These two roots,  $\Omega_l(k)$  and  $\Omega_t(k)$  (see Fig. 2.10 left), are related to the longitudinal and torsional molecular oscillations in the helix chain, respectively. The third root gives an optical branch  $\Omega_{op}(k)$  corresponding to the transverse oscillations of the molecules. At  $k = 0$ , we have

$$\Omega_{op} = \sqrt{c_{11} + c_{22} + c_{33}} = 2 \sqrt{\sum_j \alpha_j [1 - \cos(j\phi)]^2}.$$

The presence of the two acoustic branches leads to the existence of two speeds of sound: the longitudinal speed  $v_l$  and the torsional speed  $v_t$ . In the dimensionless form, they can be defined as the limits

$$s_{l,t} = v_{l,t}/v_0 = h \lim_{k \rightarrow 0} \frac{\Omega_{l,t}(k)}{k},$$

where  $v_0 = (K/M)^{1/2} R_0$  is the characteristic velocity of the small-amplitude waves in the helix macromolecule.

For the numerical helix chain dynamics simulation, we take the following parameter values:

$$\phi = 100^\circ, \quad h = 1, \quad \kappa_1 = 10, \quad \kappa_2 = 5, \quad \kappa_3 = 1. \quad (2.70)$$

The value of the angle  $\phi$  corresponds to the angular spacing of the  $\alpha$ -helix protein molecule. The rigidity constants  $k_1$ ,  $k_2$ , and  $k_3$ , approximately follow the ratios of the valence bond, angle, and hydrogen bond.

The form of the dispersion curves for the parameter set (2.70) is shown in Fig. 2.10 (left). For  $k = 0$ , the frequencies are  $\Omega_l = \Omega_t = 0$  and  $\Omega_{op} = 5.1098$ . It follows from (2.68) that there is a value of the wave number  $k = k_0 = 1.74795$  for which the free term in the dispersion equation (2.69) becomes zero. For this value, a soft torsional mode emerges  $\Omega_t(k_0) = 0$ . As can be seen from Fig. 2.10 (left), the frequency spectrum of the helix chain includes a separate optical zone and two acoustic zones, with the frequency spectrum of the torsional oscillations lying inside the frequency spectrum of the longitudinal oscillations. Moreover, the longitudinal velocity of sound  $s_l = 3.39475$  significantly exceeds the torsional velocity of sound  $s_t = 0.750411$ .

### 2.7.3 Numerical Methods for Finding the Soliton Solution

Here we consider a numerical scheme for finding solitary waves with a stationary profile, where the wave profile is found as the steady state of a certain discrete functional [42]. A necessary condition for the application of this scheme is the smooth dependence of the wave profile on the number of chain links. The main problem in applying such a scheme is finding a discrete functional that is optimal with respect to its numerical realization. To find the narrow soliton solutions, one should use the more complex pseudospectral method, suggested for one-dimensional chains by Eilbeck and Flesch [6], and used for analysis of soliton dynamics in a series of publications [7, 47, 48]. Once found, the soliton solutions are then used as the initial conditions for the numerical helix chain dynamics simulation. However, we shall demonstrate the absence of narrow solitons in the chain, so there would be no point applying the pseudospectral method, with the associated complications in its numerical realization.

The soliton solution of the equation of motion (2.61) is conveniently analysed in the cylindrical coordinate system in which

$$\begin{aligned} q_{1n} &= (1 + \eta_n) \cos(n\phi + \theta_n) , \\ q_{2n} &= (1 + \eta_n) \sin(n\phi + \theta_n) , \\ q_{3n} &= nh + \beta_n , \end{aligned}$$

where the variable  $\eta_n$  describes the radial displacement of the  $n$ th molecule from the cylinder surface, which spans all the sites of the helix chain at their equilibrium positions. The displacement is positive if a molecule is moving outside the helix and negative if it is moving inside. The second generalized coordinate  $\theta_n$  describes the azimuthal displacement of the  $n$ th molecule with respect to its equilibrium position. The third coordinate  $\beta_n$  is the  $z$  coordinate of the displacement.

In terms of the new coordinate system, the Lagrangian of the helix chain has the form

$$\begin{aligned} \mathcal{L} &= \mathcal{L} \left\{ \frac{d\eta_n}{d\tau}, \eta_n; \frac{d\theta_n}{d\tau}, \theta_n; \frac{d\beta_n}{d\tau}, \beta_n \right\} \\ &= \sum_n \left\{ \frac{1}{2} \left[ \left( \frac{d\eta_n}{d\tau} \right)^2 + (1 + \eta_n)^2 \left( \frac{d\theta_n}{d\tau} \right)^2 + \left( \frac{d\beta_n}{d\tau} \right)^2 \right] - \sum_{j=1,2,3} U_j(r_{jn}) \right\} , \end{aligned} \quad (2.71)$$

where the distance is

$$\begin{aligned} r_{jn} &= |\mathbf{q}_{n+j} - \mathbf{q}_n| \\ &= \left[ (1 + \eta_n)^2 + (1 + \eta_{n+j})^2 - 2(1 + \eta_n)(1 + \eta_{n+j}) \cos(j\phi + \theta_{n+j} - \theta_n) \right. \\ &\quad \left. + (jh + \beta_{n+j} - \beta_n)^2 \right]^{1/2} . \end{aligned}$$

The corresponding equations of motion take the form

$$\begin{aligned} \frac{d^2\eta_n}{d\tau^2} &= (1 + \eta_n) \left( \frac{d\theta_n}{d\tau} \right)^2 \\ &- \sum_{j=1,2,3} \left\{ W_j(r_{j,n-j}) \left[ 1 + \eta_n - (1 + \eta_{n-j}) \cos(j\phi + \theta_n - \theta_{n-j}) \right] \right. \\ &\quad \left. + W_j(r_{jn}) \left[ 1 + \eta_n - (1 + \eta_{n+j}) \cos(j\phi + \theta_{n+j} - \theta_n) \right] \right\} , \end{aligned} \quad (2.72)$$

$$\begin{aligned} \frac{d^2\theta_n}{d\tau^2} = \frac{1}{1+\eta_n} \Bigg\{ & -2 \frac{d\eta_n}{d\tau} \frac{d\theta_n}{d\tau} \\ & + \sum_{j=1,2,3} \left[ W_j(r_{jn})(1+\eta_{n+j}) \sin(j\phi + \theta_{n+j} - \theta_n) \right. \\ & \left. - W_j(r_{j,n-j})(1+\eta_{n-j}) \sin(j\phi + \theta_n - \theta_{n-j}) \right] \Bigg\}, \end{aligned} \quad (2.73)$$

$$\frac{d^2\beta_n}{d\tau^2} = \sum_j \left[ W_j(r_{jn})(jh + \beta_{n+j} - \beta_n) - W_j(r_{j,n-j})(jh + \beta_n - \beta_{n-j}) \right]. \quad (2.74)$$

We assume that there exists a solution in the form of a wave with a stationary profile:  $\eta_n = \eta(nh - s\tau)$ ,  $\theta_n = \theta(nh - s\tau)$ , and  $\beta_n = \beta(nh - s\tau)$ , where  $s = v/v_0$  is the dimensionless velocity. As shown in Fig. 2.10 (left), there are three types of linear modes: one optical and two acoustic modes. Therefore, there is no need to take into account the dispersion of the optical mode, and we can approximate the first and second time derivatives of the variable  $\eta_n$  by the simplest finite differences as follows:

$$\begin{aligned} \frac{d\eta_n}{d\tau} &= -s\eta'(n - s\tau) \simeq -s \frac{\eta_{n+1} - \eta_{n-1}}{2h}, \\ \frac{d^2\eta_n}{d\tau^2} &= s^2\eta''(n - s\tau) \simeq s^2 \frac{\eta_{n+1} - 2\eta_n + \eta_{n-1}}{h^2}. \end{aligned} \quad (2.75)$$

However, for the longitudinal and torsional displacements, we need to take into account the dispersion arising from the discreteness of the chain. The time derivatives of the displacements  $\theta_n$  and  $\beta_n$  require the use of a more precise finite-difference approximation. Introducing the relative displacements  $\varphi_n = \theta_{n+1} - \theta_n$  and  $\rho_n = \beta_{n+1} - \beta_n$ , we can rewrite

$$\begin{aligned} \frac{d\theta_n}{d\tau} &= -s\theta'(n - s\tau) \\ &\simeq -s \left( \frac{\theta_{n+1} - \theta_{n-1}}{2h} - \frac{\theta_{n+2} - 3\theta_{n+1} + 3\theta_n - \theta_{n-1}}{6h} \right) \\ &= s(\theta_{n+2} - 6\theta_{n+1} + 3\theta_n + 2\theta_{n-1})/6h \\ &= s(\varphi_{n+1} - 5\varphi_n - 2\varphi_{n-1})/6h, \end{aligned} \quad (2.76)$$

$$\frac{d^2\theta_n}{d\tau^2} = s^2\theta''(n - s\tau)$$



$$\begin{aligned}
&\simeq s^2 \left( \frac{\theta_{n+1} - 2\theta_n + \theta_{n-1}}{h^2} - \frac{\theta_{n+2} - 4\theta_{n+1} + 6\theta_n - 4\theta_{n-1} + \theta_{n-2}}{12h^2} \right) \\
&= -s^2(\varphi_{n+1} - 15\varphi_n + 15\varphi_{n-1} - \varphi_{n-2})/12h^2, \tag{2.77}
\end{aligned}$$

$$\begin{aligned}
\frac{d\beta_n}{d\tau} &\simeq s(\beta_{n+2} - 6\beta_{n+1} + 3\beta_n + 2\beta_{n-1})/6h \\
&= s(\rho_{n+1} - 5\rho_n - 2\rho_{n-1})/6h, \tag{2.78}
\end{aligned}$$

$$\begin{aligned}
\frac{d^2\beta_n}{d\tau^2} &= s^2\beta''(n - s\tau) \\
&\simeq -s^2(\rho_{n+1} - 15\rho_n + 15\rho_{n-1} + \rho_{n-2})/12h^2. \tag{2.79}
\end{aligned}$$

Using the finite-difference approximations (2.75)–(2.79), we rewrite the equations of motion (2.72)–(2.74) as discrete equations for the relative displacements  $\eta_n$ ,  $\varphi_n$ , and  $\rho_n$ :

$$\begin{aligned}
\mathcal{F}_{n,1} &= \frac{s^2}{h^2} \left[ \eta_{n+1} - 2\eta_n + \eta_{n-1} - (1 + \eta_n)(\varphi_{n+1} - 5\varphi_n - 2\varphi_{n-1})^2/36 \right] \\
&+ \sum_{j=1,2,3} \left\{ W_j(r_{j,n-j}) \left[ 1 + \eta_n - (1 + \eta_{n-j}) \cos \left( j\phi + \sum_{i=1}^j \varphi_{n-j+i-1} \right) \right] \right. \\
&\quad \left. + W_j(r_{jn}) \left[ 1 + \eta_n - (1 + \eta_{n+j}) \cos \left( j\phi + \sum_{i=1}^j \varphi_{n+i-1} \right) \right] \right\} = 0, \tag{2.80}
\end{aligned}$$

$$\begin{aligned}
\mathcal{F}_{n,2} &= \frac{s^2}{12h^2} \left[ (1 + \eta_n)(\varphi_{n+1} - 15\varphi_n + 15\varphi_{n-1} - \varphi_{n-2}) \right. \\
&\quad \left. + 2(\eta_{n+1} - \eta_{n-1})(\varphi_{n+1} - 5\varphi_n - 2\varphi_{n-1}) \right] \\
&+ \sum_{j=1,2,3} \left[ W_j(r_{jn})(1 + \eta_{n+j}) \sin \left( j\phi + \sum_{i=1}^j \varphi_{n+i-1} \right) \right. \\
&\quad \left. - W_j(r_{j,n-j})(1 + \eta_{n-j}) \sin \left( j\phi + \sum_{i=1}^j \varphi_{n-j+i-1} \right) \right] = 0, \tag{2.81}
\end{aligned}$$

$$\begin{aligned}
\mathcal{F}_{n,3} - \mathcal{F}_{n-1,3} = & \frac{s^2}{12h^2}(\rho_{n+1} - 15\rho_n + 15\rho_{n-1} - \rho_{n-2}) \\
& + \sum_{j=1,2,3} \left[ W_j(r_{jn}) \left( jh + \sum_{i=1}^j \rho_{n+i-1} \right) \right. \\
& \quad \left. - W_j(r_{j,n-j}) \left( jh + \sum_{i=1}^j \rho_{n-j+i-1} \right) \right] = 0 .
\end{aligned} \tag{2.82}$$

Equation (2.82) can be integrated once with the result

$$\begin{aligned}
\mathcal{F}_{n,3} = & \frac{s^2}{12h^2}(\rho_{n+1} - 14\rho_n + \rho_{n-1}) \\
& + \sum_{j=1,2,3} \sum_{l=1}^j W_j(r_{j,n-j+l}) \left( jh + \sum_{i=1}^j \rho_{n-j+l+i-1} \right) = 0 .
\end{aligned} \tag{2.83}$$

The system of the discrete equations (2.80), (2.81), and (2.83) was solved numerically. Our aim was to find the soliton solutions of this system, i.e., the solutions  $\{\eta_n, \varphi_n, \rho_n\}_{n=1}^N$  which depend smoothly on the number of chain sites  $n$ , and have asymptotic behavior at the chain ends.

The first approximation to the soliton solution can be conveniently found as the minimum of the functional

$$F = \frac{1}{2} \sum_{n=4}^{N-3} (\mathcal{F}_{n,1}^2 + \mathcal{F}_{n,2}^2 + \mathcal{F}_{n,3}^2) , \tag{2.84}$$

where  $N$  is the number of chain sites. The problem for the conditional minimum

$$\mathcal{F} \rightarrow \min : \quad \eta_n = \varphi_n = \rho_n = 0 , \quad n = 1, 2, 3, N-2, N-1, N , \tag{2.85}$$

was solved numerically using the variable metric method. The initial point was taken in the form of the bell-shaped pulse

$$\begin{aligned}
\eta_n &= A_\eta / \cosh^2 [\mu(n - N/2)] , \\
\varphi_n &= A_\varphi / \cosh^2 [\mu(n - N/2)] , \\
\rho_n &= A_\rho / \cosh^2 [\mu(n - N/2)] ,
\end{aligned}$$

where the parameter  $\mu$  describes the reciprocal width and  $A_\eta$ ,  $A_\varphi$ , and  $A_\rho$  are the amplitudes of the initial approximation to the soliton solution. The number of sites  $N$  must chosen to be approximately ten times larger than the soliton width. In this case, the soliton shape will not depend on the boundary conditions. We took  $N = 400$ , which is appropriate for finding the broad soliton solutions.

Because of surface roughness, corresponding to the functional

$$\mathcal{F} = \mathcal{F}(\eta_4, \dots, \eta_{N-3}; \varphi_4, \dots, \varphi_{N-3}; \rho_4, \dots, \rho_{N-3}) ,$$

the search for the soliton solution as a minimum of the functional (2.84) leads to a slow convergence of the numerical minimization procedure. Therefore, the final form of the solution was found as a numerical solution of the system of  $3(N-6)$  nonlinear equations (2.80), (2.81), and (2.83) with respect to the variables  $\{\eta_n, \varphi_n, \rho_n\}_{n=4}^{N-3}$ , where  $\eta_n, \varphi_n, \rho_n \equiv 0$  for  $n = 1, 2, 3, \dots, N-2, N-1, N$ . The system of nonlinear equations was solved numerically using the modified hybrid method (with the standard program from the package MINPACK). The point obtained by solving the constrained minimum problem (2.85) was used as the initial point for this method.

In addition to the velocity  $s$ , the soliton solution  $\{\eta_n, \varphi_n, \rho_n\}_{n=1}^N$  is also characterised by its energy

$$E = \sum_{n=2}^{N-1} \left\{ \frac{s^2}{8h^2} \left[ (\eta_{n+1} - \eta_{n-1})^2 + \frac{1}{9} (1 + \eta_n)^2 (\varphi_{n+1} - 5\varphi_n - 2\varphi_{n-1})^2 + \frac{1}{9} (\rho_{n+1} - 5\rho_n - 2\rho_{n-1})^2 \right] + \sum_{j=1}^3 U_j(r_{jn}) \right\} ,$$

which follows from (2.71), (2.75), (2.76), and (2.78), and the amplitudes are

$$\begin{aligned} A_\eta &= \eta_{n'} , \quad \text{where} \quad |\eta_{n'}| = \max_{1 \leq n \leq N} |\eta_n| , \\ A_\varphi &= \varphi_{n'} , \quad \text{where} \quad |\varphi_{n'}| = \max_{1 \leq n \leq N} |\varphi_n| , \\ A_\rho &= \rho_{n'} , \quad \text{where} \quad |\rho_{n'}| = \max_{1 \leq n \leq N} |\rho_n| . \end{aligned}$$

The root-mean-square width is

$$L = 2 \left[ \sum_{n=1}^N (n - n_c)^2 \rho_n / R \right]^{1/2} ,$$

where

$$R = \sum_{n=1}^N \rho_n$$

is the total compression of the helix chain and

$$n_c = \frac{1}{2} + \sum_{n=1}^N \frac{n\rho_n}{R}$$

is the position of the soliton center.

### 2.7.4 Results of Numerical Analysis

Let us find the soliton solutions for the chain with parameters (2.70). The nonlinearity of the dynamics observed in  $\alpha$ -chain protein macromolecules is caused mainly by their three-dimensional geometry and the nonlinearity of the soft hydrogen bonds. Therefore, we take into account the nonlinearity of the interaction only between distant neighbors, i.e., we set  $\gamma_1 = 0$ ,  $\gamma_2 = 0$ , and  $\gamma_3 \geq 0$ . To distinguish between the effects of the geometrical and physical anharmonicity on the chain nonlinear dynamics, we consider the soliton solutions for the four values of the anharmonicity  $\gamma_3 = 0, 0.1, 1$ , and  $10$ . For  $\gamma_3 = 0$ , physical anharmonicity is absent and the nonlinear dynamics is defined by the geometrical anharmonicity of the chain. As the value of  $\gamma_3$  increases, the geometrical anharmonicity effect decreases, while the physical anharmonicity effect increases.

The numerical analysis performed for the discrete system of (2.80), (2.81), and (2.83) showed that two types of acoustic solitons can exist in the helix chain: solitons of torsion and compression. The torsional soliton is a localized nonlinear packet of torsional phonons, moving with the supersonic velocity  $s > s_t$ . The compression soliton is a localized nonlinear packet of longitudinal phonons moving with the supersonic velocity  $s > s_l$ .

The form of the torsional soliton is shown in Fig. 2.10 (right). The soliton has a bell-shaped profile in all three coordinates  $\eta_n$ ,  $\varphi_n$ , and  $\rho_n$ . In a region of soliton localization, untwisting of the helix chain occurs ( $\varphi_n > 0$ ). The radius of the helix chain decreases ( $\eta_n < 0$ ) and its length increases ( $\rho_n > 0$ ). The existence of the soliton is associated with the geometrical anharmonicity. The physical anharmonicity has the opposite sign and so opposes the formation of the torsion soliton. An increase in the physical anharmonicity parameter, i.e.,  $\gamma_3 \geq 0$ , leads to narrowing of the soliton velocity spectrum. With weak physical anharmonicity ( $\gamma_3 = 0, 0.1$ ), the spectrum of the soliton velocity is  $1 < s/s_t < 1.59$ . With medium physical anharmonicity ( $\gamma_3 = 1$ ), the spectrum is narrower by a factor of two, viz.,  $1 < s/s_t < 1.32$ , and with strong physical anharmonicity ( $\gamma_3 = 10$ ), the torsional soliton no longer exists in the helix chain (the physical anharmonicity is stronger than the geometrical anharmonicity).

The numerical simulation showed that the soliton's motion is always accompanied by phonon emission (see Fig. 2.10 right). This emission is considerably more intensive at the maximal velocity. As a result of the emission, the energy and the velocity of the soliton steadily decrease (see Fig. 2.11 left). The energy  $E$  and the velocity  $s$  of the soliton depend on the time  $\tau$ . To estimate emission intensity, it is

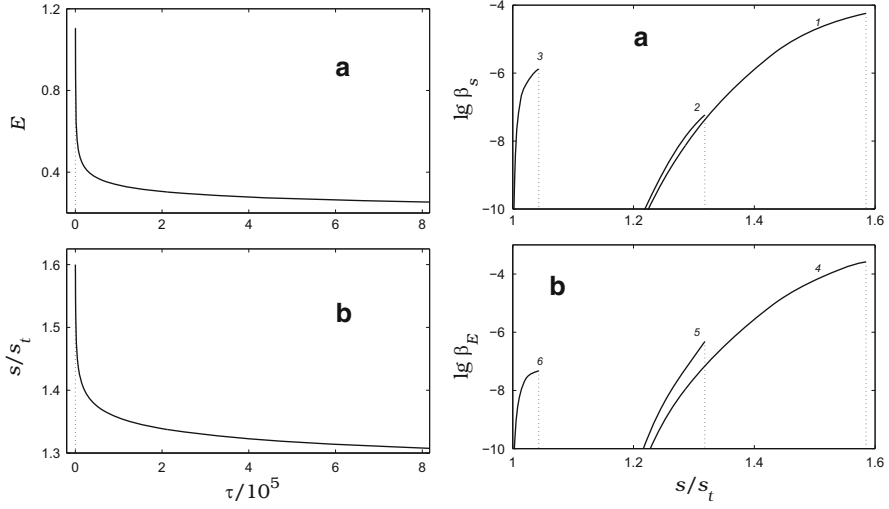


**Fig. 2.11** *Left:* Dependence of the energy  $E$  and velocity  $s$  of the torsion soliton on the dimensionless time  $\tau$ . The anharmonicity parameter is  $\gamma_3 = 0$ . *Right:* Dependence of the relaxation coefficients of the velocity  $\beta_s$  and energy  $\beta_E$  of the torsion soliton on its velocity  $s$  for  $\gamma_3 = 0$  (lines 1 and 4) and  $\gamma_3 = 1$  (lines 2 and 5). Dependence of the relaxation coefficients for the localized breather-like state at  $\gamma_3 = 10$  (lines 3 and 6)

convenient to define the relaxation coefficients  $\beta_s = -s'/s_t$  and  $\beta_E = -E'/E$ , where the prime denotes differentiation with respect to  $\tau$ . As the soliton shape is uniquely determined by its velocity  $s$ , the relaxation coefficients  $\beta_s$  and  $\beta_E$  also uniquely depend on  $s$ . When the soliton velocity  $s$  decreases, the intensity of phonon emission tends exponentially to zero and becomes negligibly small at  $s = 1.22s_t$  (see Fig. 2.11 right). At velocities  $1 < s/s_t < 1.22$ , the phonon emission vanishes completely and the soliton moves with a constant velocity.

With an increase in soliton velocity, its energy  $E$  and the absolute values of its three amplitudes  $A_\eta$ ,  $A_\varphi$ , and  $A_\rho$  increase steadily, while its width  $L$  decreases monotonically (see Table 2.2). At  $s/s_t < 1.2$ , its width significantly exceeds the chain spacing that allows the use of the continuum approximation. The discreteness effects of the helix chain become apparent through the noticeable phonon emission at higher velocities. These effects manifest themselves more strongly as the soliton width decreases.

With strong physical anharmonicity ( $\gamma_3 = 10$ ), the torsion soliton does not exist. The numerical simulation showed that, instead of the torsion soliton, there is a localized breather-like excitation (see Fig. 2.12 left), which has a narrow velocity spectrum  $1 < s/s_t < 1.043$ . The helix chain twisting occurs in the excitation localization region ( $\varphi_n < 0$ ), decreasing its length ( $\rho_n < 0$ ) and increasing its radius ( $\eta_n > 0$ ). The motion of the excitation is also accompanied by phonon emission. With decreasing excitation velocity, the emission intensity tends exponentially to zero (see Fig. 2.11 right).

**Table 2.2** Dependence of the energy  $E$ , width  $L$ , amplitudes  $A_\eta$ ,  $A_\varphi$ , and  $A_\rho$ , and transmission coefficient  $p$  of the torsion soliton in the helix chain on its velocity  $s$  for  $\gamma_3 = 1$

$s/s_t$	$E$	$L$	$A_\eta$	$A_\varphi$	$A_\rho$	$p$
1.04	0.01016	14.17	-0.0194	0.0363	0.0185	$0.643 \pm 0.020$
1.08	0.03117	10.54	-0.0385	0.0735	0.0364	$0.463 \pm 0.020$
1.12	0.06247	9.25	-0.0576	0.1121	0.0543	$0.347 \pm 0.018$
1.16	0.10585	9.11	-0.0770	0.1531	0.0727	$0.269 \pm 0.016$
1.20	0.16499	9.06	-0.0976	0.1966	0.0916	$0.216 \pm 0.014$

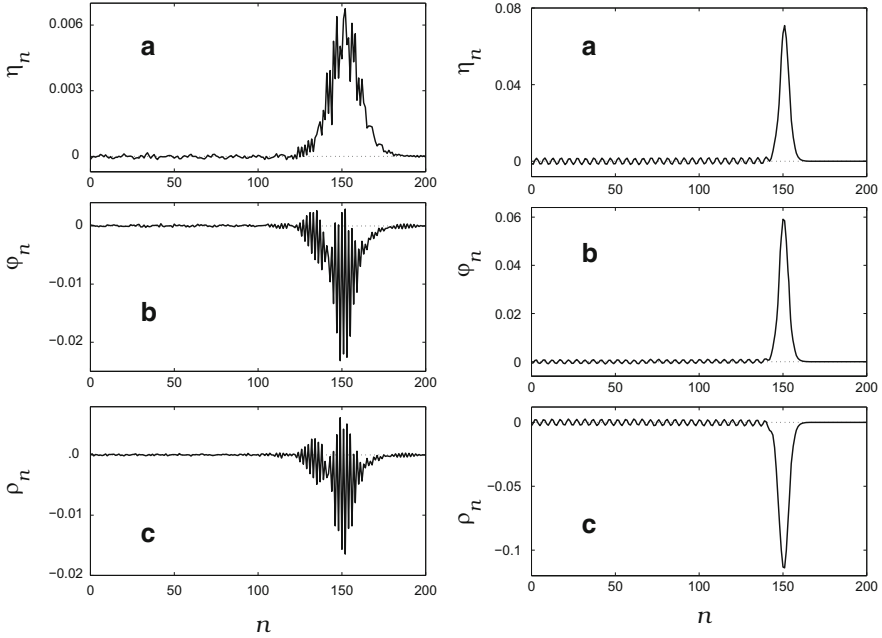


**Fig. 2.12** *Left:* The three-component profile of the breather-like excitation at velocity  $s = 1.042s_t$  ( $\gamma_3 = 10$ ). *Right:* The three-component profile of the compression soliton at velocity  $s = 1.146s_1$  ( $\gamma_3 = 1$ ). Phonon emission by the soliton is clearly visible

The profile of the compression soliton is shown in Fig. 2.12 (right). The soliton has a bell-shaped profile in all three coordinates  $\eta_n$ ,  $\varphi_n$ , and  $\rho_n$ . In the soliton localization region, compression ( $\rho_n < 0$ ) and slight untwisting of the helix chain ( $\varphi_n > 0$ ) occur, these being accompanied by an increase in the helix chain radius ( $\eta_n > 0$ ). The existence of the compression soliton is associated with the physical anharmonicity. In the absence of physical anharmonicity ( $\gamma_3 = 0$ ), the soliton does not exist. The spectrum of soliton velocities broadens steadily when the anharmonicity parameter is increased. Thus, for  $\gamma_3 = 0.1$ , the soliton velocity spectrum is  $1 < s/s_1 < 1.065$ , while for  $\gamma_3 = 1$ , it is twice as broad  $1 < s/s_1 < 1.143$ . A further increase in the anharmonicity parameter does not lead

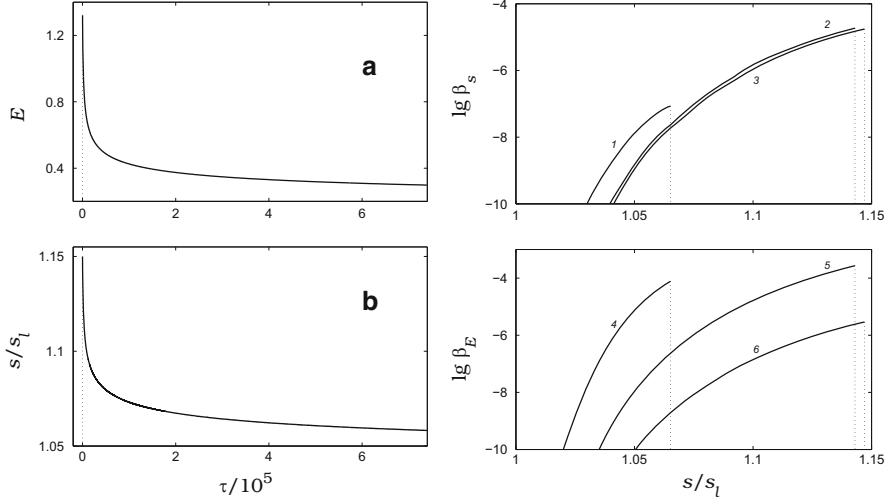


**Fig. 2.13** *Left:* Dependence of the energy  $E$  and the velocity  $s$  on the dimensionless time  $\tau$ . The anharmonicity parameter is  $\gamma_3 = 1$ . *Right:* Dependence of the relaxation coefficients of the velocity  $\beta_s$  and the energy  $\beta_E$  for the compression soliton on its velocity  $s$  for  $\gamma_3 = 0.1$  (lines 1 and 4),  $\gamma_3 = 1$  (lines 2 and 5), and  $\gamma_3 = 10$  (lines 3 and 6)

to a significant change in the velocity spectrum: the spectrum is  $1 < s/s_l < 1.147$  for  $\gamma_3 = 10$ .

The numerical simulation of the soliton dynamics showed that the soliton motion is always accompanied by phonon emission (see Fig. 2.12 right). This emission is more intensive at its maximal velocity. As a result of the emission, the energy and the velocity of the soliton both decrease monotonically (see Fig. 2.13 left). We define the velocity relaxation coefficient as  $\beta_s = -s'/s_l$ . When the soliton velocity  $s$  decrease, the phonon emission intensity tends exponentially to zero (see Fig. 2.13 right). As can be seen, phonon emission is completely absent for  $s/s_l < 1.02$  when  $\gamma_3 = 0.1$ ,  $s/s_l < 1.035$  when  $\gamma_3 = 1$ , and  $s/s_l < 1.05$  when  $\gamma_3 = 10$ .

When the soliton velocity  $s$  decreases, its energy  $E$  and the absolute values of all three coordinates  $A_\eta$ ,  $A_\varphi$ , and  $A_\rho$  increase steadily, while its width  $L$  decreases monotonically (see Table 2.3). As can be seen, for  $1 < s/s_l < 1.05$ , the soliton width significantly exceeds the chain spacing. Comparing Tables 2.2 and 2.3, we may conclude that the helix chain deformation in the torsion soliton localization region is caused mainly by its untwisting, while in the compression soliton localization region, it is due to its longitudinal compression.

**Table 2.3** Dependence of the energy  $E$ , width  $L$ , amplitudes  $A_\eta$ ,  $A_\varphi$ , and  $A_\rho$ , and transmission coefficient  $p$  of the compression soliton on its velocity  $s$  for  $\gamma_3 = 1$

$s/s_1$	$E$	$L$	$A_\eta$	$A_\varphi$	$A_\rho$	$p$
1.01	0.02022	20.78	0.0054	0.0049	-0.0093	$0.814 \pm 0.020$
1.02	0.05763	15.18	0.0107	0.0096	-0.0183	$0.708 \pm 0.020$
1.03	0.10670	12.55	0.0158	0.0143	-0.0271	$0.627 \pm 0.018$
1.04	0.16557	11.03	0.0208	0.0188	-0.0358	$0.560 \pm 0.016$
1.05	0.23329	10.03	0.0258	0.0232	-0.0441	$0.506 \pm 0.014$

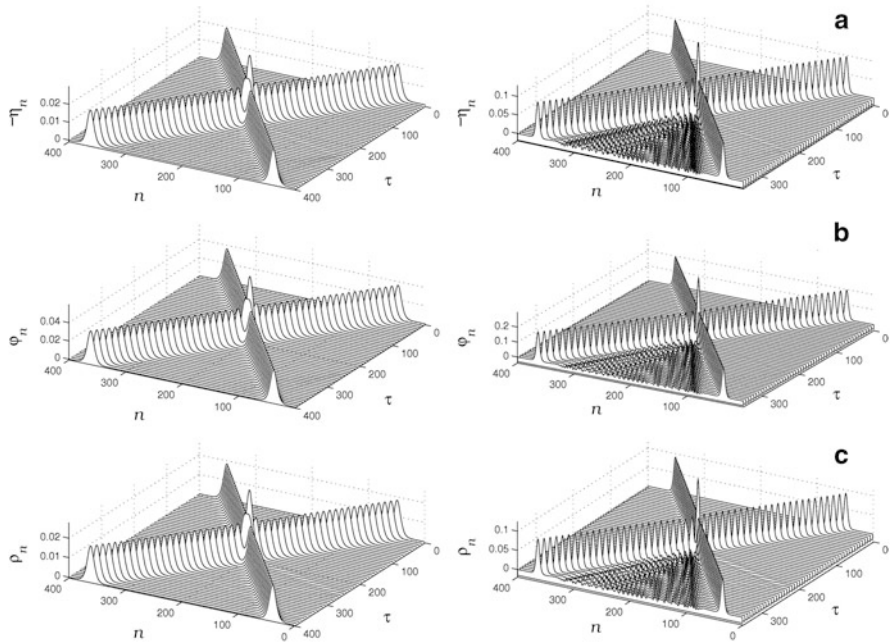


**Fig. 2.14** *Left*: Elastic collision of two torsion solitons. The velocities of the first and second solitons are  $s_1 = 1.04s_1$  and  $s_2 = -1.04s_1$ , respectively ( $\gamma_3 = 1$ ). *Right*: Inelastic collision of two torsion solitons. The velocities of the first and second solitons are  $s_1 = 1.2s_1$  and  $s_2 = -1.2s_1$ , respectively ( $\gamma_3 = 1$ )

### 2.7.5 Soliton Interaction

At velocities close to the sound velocity  $s_1$ , torsion solitons interact with each other as elastic particles. Their collision leads to elastic repulsion without phonon emission and a change of shape (see Fig. 2.14 left). At higher velocities, the soliton interaction becomes inelastic, and the collision is accompanied by phonon emission (see Fig. 2.14 right). Compression solitons moving with a velocity close to the speed of sound  $s_1$  also interact as elastic particles. For other velocity values, the soliton



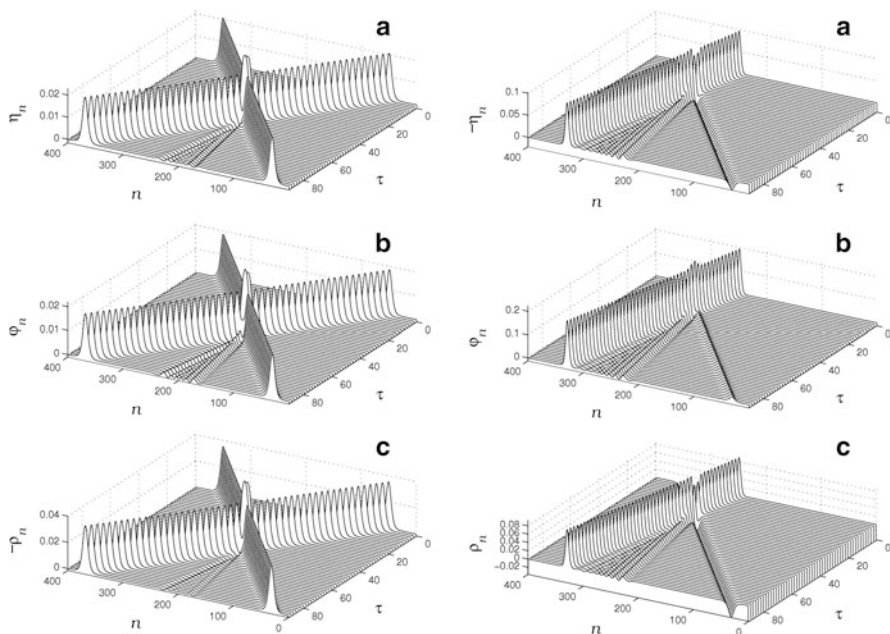


**Fig. 2.15** *Left*: Inelastic collision of two compression solitons. The velocities of the first and second solitons are  $s_1 = 1.04s_l$  and  $s_2 = -1.04s_l$ , respectively ( $\gamma_3 = 1$ ). *Right*: Inelastic collision of a torsion soliton (velocity  $s_1 = 1.2s_l$ ) with a compression soliton (velocity  $s_2 = -1.04s_l$ ). The anharmonicity parameter is  $\gamma_3 = 1$

repulsion is accompanied by torsional phonon emission (see Fig. 2.15 left). Solitons of different types interact with each other as inelastic particles. Even at velocities close to  $s_t$  and  $s_l$ , their collision leads to inelastic repulsion followed by phonon emission. The greater the velocity, the more intensive the emission (see Fig. 2.15 right). This way, both types of acoustic solitons interact with each other as elastic particles in the helix molecule. A soliton collision leads to their repulsion, followed by nonessential phonon emission.

### 2.7.6 Modeling Acoustic Soliton Formation

In finite helix chains, acoustic solitons can be formed by deformation of chain end-links. Here we model this process. Consider the chain dynamics under the torsion deformation of three chain end-links. We integrate the equations of motion (2.72)–(2.74) with fixed end boundary conditions  $\eta'_n \equiv 0$ ,  $\theta'_n \equiv 0$ , and  $\beta'_n \equiv 0$  for  $n = 1, \dots, N$  and the following initial conditions:

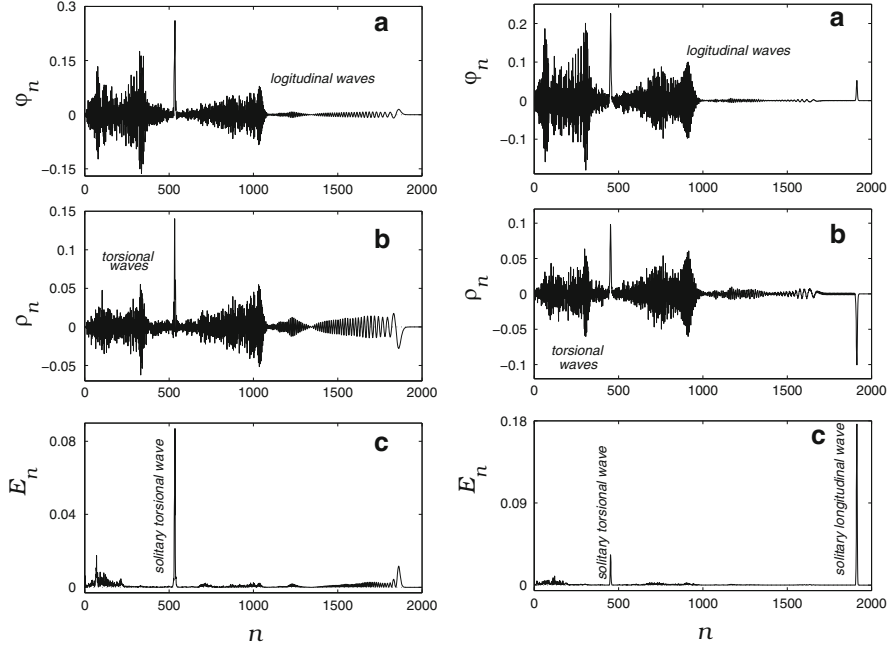


**Fig. 2.16** *Left:* Formation of the torsion soliton and two wave packets in the helix chain under untwisting of three chain end-links at the initial time ( $\tau = 0$ ). The amplitude of the initial deformation is  $A_\theta = \pi/2$  and the anharmonicity parameter is  $\gamma_3 = 0$ . The distributions of the relative angular deformation  $\varphi_n$ , relative displacement  $\rho_n$ , and energy  $E_n$  in the helix chain at time  $\tau = 550$  are shown. *Right:* Formation of a torsion soliton, compression soliton, and two wave packets in the helix chain under untwisting of three chain end-links at the initial time ( $\tau = 0$ ). The amplitude of the initial deformation is  $A_\theta = \pi/2$  and the anharmonicity parameter is  $\gamma_3 = 0$ . The distributions of the relative angular deformation  $\varphi_n$ , relative displacement  $\rho_n$ , and energy  $E_n$  in the helix chain at time  $\tau = 550$  are shown

$$\begin{aligned} \eta_n(0) = 0, \quad \eta'_n(0) = 0, \quad \beta_n(0) = 0, \quad \beta'_n(0) = 0, \quad n = 1, 2, \dots, N, \\ \theta_1(0) = \theta_2(0) = \theta_3(0) = -A_\theta, \quad \theta_n(0) = 0, \quad \theta'_n(0) = 0, \quad n = 4, \dots, N, \end{aligned}$$

where  $A_\theta$  is the amplitude of the torsional deformation and  $N = 2,000$  is the number of chain sites.

Numerical simulation of the dynamics has shown that initial deformation of the chain end-links leads to the formation of two oscillating wave packets and a torsion soliton in the chain for  $\gamma_3 = 0$  (see Fig. 2.16 left). For the deformation amplitude  $A_\theta = -\pi/2$ , the torsion soliton accumulates more than 20 % of the initial deformation energy. For  $\gamma_3 = 1$ , the chain end-link deformation leads to the formation of two acoustic solitons (see Fig. 2.16 right). The torsion and compression solitons accumulate 9 and 48 % of initial deformation energy, respectively. The rest of the energy is spent on the formation of a wave packet of torsion solitons.

**Table 2.4** Dimensional  $M_k$  (given in proton mass) and dimensionless  $\mu_k$  masses of 20 amino acid residues of an  $\alpha$ -helix protein molecule

Notation	Gly	Ala	Val	Leu	Ile	Phe	Pro
$M$	57	71	99	113	113	147	125
$\mu$	0.474	0.591	0.824	0.940	0.940	1.223	1.040
Notation	Trp	Ser	Thr	Met	Asn	Gln	Cys
$M$	186	87	101	131	114	128	103
$\mu$	1.548	0.724	0.841	1.090	0.949	1.065	0.857
Notation	Asp	Glu	Tyr	His	Lys	Arg	Average
$M$	115	129	163	137	128	156	120.15
$\mu$	0.957	1.074	1.357	1.140	1.065	1.298	1

The dynamics simulation carried out showed that the torsional deformation of the three chain end-links can be an effective mechanism of acoustic soliton initiation in a helix macromolecule. The effectiveness of the initiation can exceed 50 %.

### 2.7.7 Interaction of Solitons with Molecular Chain Heterogeneities

All protein molecules consist of 20 types of amino acids, each with a different mass (see Table 2.4). Therefore, in an  $\alpha$ -helix chain macromolecule, the mass of each link depends on its number. Let us consider the acoustic soliton dynamics in a chain with a random distribution of amino acid residues.

Values of the mass  $\{M_k\}_{k=1}^{20}$  of amino acid residues are given in Table 2.4. The average mass value is

$$\overline{M} = \frac{1}{20} \sum_{k=1}^{20} M_k = 120.15 m_p ,$$

where  $m_p$  is the proton mass. Introducing the dimensionless masses  $\mu_k = M_k / \overline{M}$ , the equations of motion (2.72)–(2.74) of the helix chain take the form

$$\begin{aligned}
 m_n \frac{d^2 \eta_n}{d\tau^2} = & m_n (1 + \eta_n) \left( \frac{d\theta_n}{d\tau} \right)^2 \\
 & - \sum_{j=1,2,3} \left\{ W_j(r_{j,n-j}) \left[ 1 + \eta_n - (1 + \eta_{n-j}) \cos(j\phi + \theta_n - \theta_{n-j}) \right] \right. \\
 & \left. + W_j(r_{jn}) \left[ 1 + \eta_n - (1 + \eta_{n+j}) \cos(j\phi + \theta_{n+j} - \theta_n) \right] \right\} ,
 \end{aligned}
 \tag{2.86}$$

$$\begin{aligned}
m_n \frac{d^2 \theta_n}{d\tau^2} = \frac{1}{1 + \eta_n} \left\{ -2m_n \frac{d\eta_n}{d\tau} \frac{d\theta_n}{d\tau} \right. \\
+ \sum_{j=1,2,3} \left[ W_j(r_{jn})(1 + \eta_{n+j}) \sin(j\phi + \theta_{n+j} - \theta_n) \right. \\
\left. \left. - W_j(r_{j,n-j})(1 + \eta_{n-j}) \sin(j\phi + \theta_n - \theta_{n-j}) \right] \right\}, \quad (2.87)
\end{aligned}$$

$$m_n \frac{d^2 \beta_n}{d\tau^2} = \sum_j \left[ W_j(r_{jn})(jh + \beta_{n+j} - \beta_n) - W_j(r_{j,n-j})(jh + \beta_n - \beta_{n-j}) \right], \quad (2.88)$$

where the mass  $m_n$  of the  $n$ th link can take any of the 20 values  $\{\mu_k\}_{k=1}^{20}$  with equal probability.

Let us consider a chain of  $N = 2,000$  links, where the first and the last 500 chain links have equal masses:  $m_n = 1$ ,  $n = 1, \dots, 500$ ,  $n = 1,501, \dots, 2,000$ . The masses of the links with numbers  $500 < n \leq 1,500$  are randomly chosen from the 20 dimensionless values  $\{\mu_k\}_{k=1}^{20}$ . To model the passage through this inhomogeneous region of the chain by an acoustic soliton, we integrate the equations of motion (2.86)–(2.88) with initial conditions corresponding to the acoustic soliton centered at  $n_c = 50$ .

The example of the passage of the soliton through the inhomogeneous region of the chain is shown in Fig. 2.17. We observe that the helix chain inhomogeneities

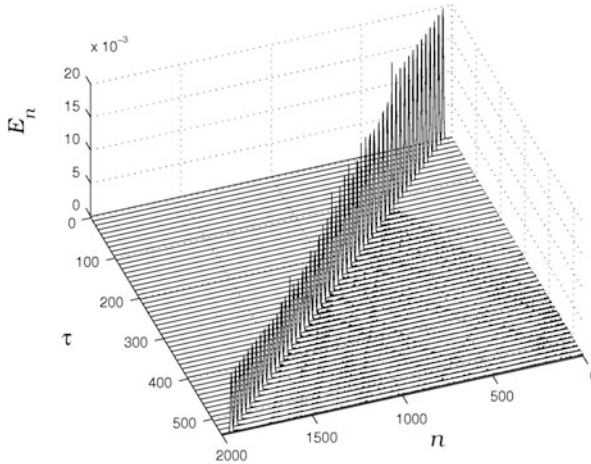


**Fig. 2.17** Passage of a compression soliton through an inhomogeneous region of the helix chain. Dependence of energy  $E_n$  over the chain on time  $\tau$ . Initial soliton velocity  $s = 1.05s_1$ , anharmonicity parameter  $\gamma_3 = 1$ , and transmission coefficient  $p = 0.557$

do not cause the soliton to collapse. The soliton only emits phonons, thus leading to energy loss. We introduce the transmission coefficient  $p = E_t/E_i$ , where  $E_i$  is the initial energy of the soliton and  $E_t$  is its energy after passage through an inhomogeneous region of the helix chain. The value of  $p$  was estimated from the results of 100 independent computational experiments.

The dependences of the transmission coefficient  $p$  on the torsion velocity and the compression solitons are given in Tables 2.2 and 2.3, respectively. We observe that the energy loss grows steadily with the soliton velocity. The compression soliton is more stable with respect to the chain inhomogeneities than the torsion soliton. The simulation shows that the acoustic compression soliton can be an effective energy carrier in an  $\alpha$ -helix macromolecule for a distance of up to 1,000 chain spacings.

## 2.8 Conclusion

The investigation undertaken shows that two types of acoustic solitons can exist in a helix chain: the soliton of torsion and the soliton of compression. The torsion soliton is a localized nonlinear packet of torsional phonons with velocity higher than the velocity of sound of torsional phonons in the helix chain. The soliton describes the motion of a localization region of helix untwisting along the chain (in the soliton localization region, the helix chain stretches and its radius decreases). The compression soliton is a localized nonlinear packet of longitudinal phonons with velocity higher than the longitudinal sound velocity in the helix chain (in the localization region of the soliton, the helix chain also slightly stretches and its radius increases). The existence of the torsion soliton is associated with the geometrical anharmonicity, while the compression soliton is defined by the physical anharmonicity (the molecular interaction anharmonicity) of the helix chain.

Solitons interact with each other as elastic particles. Their collision leads to reflection, followed by slight phonon emission. In a finite chain, the solitons can be formed as a result of the torsional deformation of three chain end-links. The effectiveness of such initiation of the soliton can exceed 50 %.

If the soliton interacts with inhomogeneities in the  $\alpha$ -helix chain, this does not cause immediate soliton collapse. The soliton only emits phonons when it passes through the inhomogeneity, leading to energy loss. The compression soliton is more stable with respect to chain inhomogeneities than the torsion soliton. It can serve as an effective energy carrier for a distance of up to 1,000 chain spacings.

## References

1. Fermi, E., Pasta, J., Ulam, S.: Studies of nonlinear problems, I. Los Alamos Report LA 1940 (1955)
2. Zabusky, N.J., Deem, G.S.: Dynamics of nonlinear lattices. Localized optical excitations, acoustic radiations and strong nonlinear behavior. J. Comput. Phys. 2, 207 (1968)

3. Zabusky, N.J.: Nonlinear lattice dynamics and energy sharing. *J. Phys. Soc. Jpn. Suppl.* **26**, 196 (1969)
4. Zabusky, N.J., Kruskal, M.D.: Interaction of solitons in a collisionless plasma and the recurrence of initial states. *Phys. Rev. Lett.* **15**(6), 240 (1965)
5. Toda, M., Waddati, M.A.: Solitons and two solitons in an exponential lattice and related equation. *J. Phys. Soc. Jpn.* **34**, 18 (1973)
6. Eilbeck, J.C., Flesh, R.: Calculation of families of solitary waves on discrete lattices. *Phys. Lett. A* **149**, 200 (1990)
7. Duncan, D.B., Eilbeck, J.C., Feddersen, H., Wattis, J.A.D.: Solitons on lattices. *Physica D* **68**, 1 (1993)
8. Toda, M.: *Theory of Nonlinear Lattices*, 2nd edn. Springer, Berlin (1989)
9. Toda, M.: Vibration of a chain with nonlinear interaction. *J. Phys. Soc. Jpn.* **22**, 431 (1967)
10. Toda, M.: Wave propagation in anharmonic lattices. *J. Phys. Soc. Jpn.* **23**, 501 (1967)
11. Toda, M.: Wave in nonlinear lattices. *Prog. Theor. Phys. Suppl.* **45**, 174 (1970)
12. Toda, M.: Studies of a nonlinear lattice. *Phys. Rep. C* **18**, 1 (1975)
13. Toda, M.: Solitons and heat conduction. *Phys. Scr.* **20**, 424 (1979)
14. Mokross, F., Buttner, H.: Thermal conductivity in the diatomic Toda lattice. *J. Phys. C Solid State Phys.* **16**, 4539 (1983)
15. Jackson, E., Mistriotis, F.: Thermal conductivity of one- and two-dimensional lattices. *J. Phys. C Condens. Matter.* **1**, 1223 (1989)
16. Newell, A.C.: *Solitons in Mathematics and Physics*. Society for Industrial and Applied Mathematics, Philadelphia (1985)
17. Narayamurti, V., Varma, S.: Nonlinear propagation of heat pulses in solids. *Phys. Rev. Lett.* **25**, 1105 (1970)
18. Mertens, F.G., Buttner, H.: *Modern Problems in Condensed Matter Sciences*, vol. 17. North-Holland, Amsterdam (1986)
19. Gendelman, O.V., Manevich, L.I.: Exact soliton-like solutions in generalised dynamical models of quasi-one-dimensional crystal. *Sov. Phys. JETP* **102**, 511 (1992)
20. Bishop, A.R.: Solitons and physical perturbations. In: Lanngren, K. and Scott, A. (eds.) *Solutions in Action*. Academic Press, New York (1978)
21. Collins, M.A.: A quasicontinuum approximation for solitons in an atomic chain. *Chem. Phys. Lett.* **77**, 342 (1981)
22. Collins, M.A.: Solitons and nonlinear phenomena. *Adv. Chem. Phys.* **53**, 225 (1983)
23. Kosevich, A.M.: *Theory of Crystal Lattice*. Vishcha Shkola, Kharkov (1988)
24. Davydov, A.S.: *Solitons in Molecular Systems*. Naukova Dumka, Kiev (1988)
25. Zabusky, N.J.: Solitons and energy transport in nonlinear lattices. *Comput. Phys. Commun.* **5**, 1 (1973)
26. Olsen, O.H., Lomdhal, P.S., Kerr, W.C.: Localized excitations in a three-dimensional nonlinear model. *Phys. Lett. A* **136**, 402 (1989)
27. Christiansen, P.L., Lomdhal, P.S., Muto, V.: On a Toda lattice model with a transversal degree of freedom. *Nonlinearity* **4**, 477 (1990)
28. Muto, V., Lomdhal, P.S., Christiansen, P.L.: Two-dimensional discrete model for DNA dynamics: longitudinal wave propagation and denaturation. *Phys. Rev. A* **42**, 7452 (1990)
29. Lomdhal, P.S., Olsen, O.H., Samuelsen, M.R.: Transverse instabilities in a three-dimensional non-linear chain. *Phys. Lett. A* **152**, 343 (1991)
30. Turitsyn, S.K.: Blow-up in the Boussinesq equation. *Phys. Rev. E* **47**, R796 (1993)
31. Flytzanis, N., Savin, A.V., Zolotaryuk, Y.: Soliton dynamics in a thermalized molecular chain with transversal degree of freedom. *Phys. Lett. A* **193**, 148 (1994)
32. Zolotaryuk, Y., Savin, A.V.: Interaction of the acoustic soliton with transversal thermal vibrations of molecules in a chain. *Ukr. Fiz. Zh. (Ukr. Phys. J.)* **39**, 1051 (1994)
33. Savin, A.V., Zolotaryuk, Y.: The lattice soliton in a chain with orientational thermal vibrations. *Phys. Lett. A* **201**, 213 (1995)
34. Peyrard, M., Bishop, A.R.: Statistical mechanics of a nonlinear model for DNA denaturation. *Phys. Rev. Lett.* **62**, 2755 (1989)

35. Peyrard, M., Dauxois, T., Hoyet, H., Willis, C.R.: Biomolecular dynamics of DNA: statistical mechanics and dynamical models. *Physica D* **68**, 104 (1993)
36. Dauxois, T., Peyrard, M., Bishop, A.R.: Entropy-driven DNA denaturation. *Phys. Rev. E* **47**, R44 (1993)
37. Yakushevich, L.V.: *Nonlinear Physics of DNA*. Wiley, New York (1988)
38. Netrebko, N.V., Romanovsky, Y.A., Shidlovskaya, E.G.: Stochastic cluster dynamics of macromolecules. *Izvestia Vuzov* **2**, 26 (1994)
39. Romanovsky Yu.M.: Some problems of cluster dynamics of biological macromolecules. *Lect. Notes Phys.* **484**, 140 (1997)
40. Zolotaryuk, A.V., Christiansen, P.L., Savin, A.V.: Two-dimensional dynamics of a free molecular chain with a secondary structure. *Phys. Rev. E* **54**, 3881 (1996)
41. Manevich, L.I., Savin, A.V.: Solitons of tension in polyethylene molecules. *Polym. Sci. Ser. A* **38**, 789 (1996)
42. Christiansen, P.L., Savin, A.V., Zolotaryuk, A.V.: Soliton analysis in complex molecular systems: a zig-zag chain. *J. Comput. Phys.* **134**, 108 (1997)
43. Manevitch, L.I., Savin, A.V.: Solitons in crystalline polyethylene: isolated chains in the transconformation. *Phys. Rev. E* **55**, 4713 (1997)
44. Savin, A.V., Manevich, L.I., Christiansen, P.L., Zolotaruk, A.V.: Nonlinear dynamics of zigzag molecular chains. *Physics-Uspekhi* **42**, 245 (1999)
45. Christiansen, P.L., Zolotaryuk, A.V., Savin, A.V.: Solitons in an isolated helix chain. *Phys. Rev. E* **56**, 877 (1997)
46. Cadet, S.: Transverse envelope solitons in an atomic chain. *Phys. Rev. Lett.* **121**, 77 (1987)
47. Zolotaryuk, Y., Eilbeck, J.C., Savin, A.V.: Bound states of lattice solitons and their bifurcations. *Physica D* **108**, 81 (1997)
48. Savin, A.V., Zolotaryuk, Y., Eilbeck, J.C.: Moving kinks and nanopterons in the nonlinear Klein–Gordon lattice. *Physica D* **138**, 267 (2000)

Synergetics of Molecular Systems

Lupichev, L.N.; Savin, A.V.; Kadantsev, V.N.

2015, VIII, 332 p. 135 illus., Hardcover

ISBN: 978-3-319-08194-6